Ab initio derivation of multi-orbital extended Hubbard model for molecular crystals

Masahisa Tsuchiizu, Yukiko Omori, and Yoshikazu Suzumura
Department of Physics, Nagoya University, Nagoya 464-8602, Japan

Marie-Laure Bonnet
Institute of Physical Chemistry, University of Zurich, Winterthurerstrasse 190, 8057 Zurich, Switzerland

Vincent Robert
Université de Lyon, Laboratoire de Chimie, Ecole Normale Supérieure de Lyon, CNRS, 46 allée d'Italie, F-69364 Lyon, France and
Laboratoire de Chimie Quantique, UMR 7177 CNRS/Université de Strasbourg, 4, rue Blaise Pascal F-67000 Strasbourg, France
(Dated: January 30, 2012)

From configuration interaction (CI) *ab initio* calculations, we derive an effective two-orbital extended Hubbard model based on the gerade (g) and ungerade (u) molecular orbitals (MOs) of the charge-transfer molecular conductor (TTM-TTP)I_3 and the single-component molecular conductor [Au(tmdt)$_2$]. First, by focusing on the isolated molecule, we determine the parameters for the model Hamiltonian so as to reproduce the CI Hamiltonian matrix. Next, we extend the analysis to two neighboring molecule pairs in the crystal and we perform similar calculations to evaluate the inter-molecular interactions. From the resulting tight-binding parameters, we analyze the band structure to confirm that two bands overlap and mix in together, supporting the multi-band feature. Furthermore, using a fragment decomposition, we derive the effective model based on the fragment MOs and show that the staking TTM-TTP molecules can be described by the zig-zag two-leg ladder with the inter-molecular transfer integral being larger than the intra-fragment transfer integral within the molecule. The inter-site interactions between the fragments follow a Coulomb law, supporting the fragment decomposition strategy.

I. INTRODUCTION

In the long history of research on molecular solids, various materials have been synthesized and a rich variety of phenomena have been discovered, e.g., Peierls insulator, Mott insulator, charge-ordered state, antiferromagnetic state, spin and charge density wave state, and superconducting state.[1,2] For the description of almost all these phases, it has been recognized that only one frontier orbital, the highest-occupied-molecular orbital (HOMO) or lowest-unoccupied-molecular orbital (LUMO) plays a crucial role.[3,4] The tight-binding approach, where a molecule is regarded as a single site and the various ways of molecular packing are reflected by the anisotropy of inter-site transfer integrals and of inter-site Coulomb repulsions, has been successful in the systematic understanding of the origin of various phases.

Recently theoretical efforts have been devoted to accurate derivation of the single-orbital Hubbard Hamiltonian from density-functional theory (DFT; Refs. 5–10) and wavefunction-based calculations.[11–13] The magnitude of the bare "on-site" Coulomb interaction within the same molecular orbital (MO) of the benchmark TTF molecule was evaluated as ~ 5.9 eV, which is reduced to 4.7 eV by taking into account the intra-molecular screening effects.[5] The on-site Coulomb repulsion is further reduced for larger molecules, as expected, e.g., in BEDT-TTF molecule[6,7] where it is estimated ~ 4.2 eV. It is generally expected that the intra-molecular screening effects are not so pronounced for larger molecules due to the nature of delocalized molecular orbitals.[5,13] The inter-molecular screening effects have also been analyzed by several approaches.[5–8,10]

Multi-molecular-orbital properties have attracted recent attention in the single-component molecular solids,[14–16] such as [Ni(tmdt)$_2$] and [Au(tmdt)$_2$]. Among these single-component molecular solids, the metallic behavior was first confirmed in [Ni(tmdt)$_2$].[17,18] In [Au(tmdt)$_2$], antiferromagnetic ordering was observed with high transition temperature $T_{\rm AF} = 110$ K.[19–21] Interestingly, it has been proposed that in [Au(tmdt)$_2$], a new type of antiferromagnetic state, called the *intra-molecular* antiferromagnetic (IAF) state, is realized, in which two ligands within each molecule have opposite spins.[22,23] From DFT-based *ab initio* calculations for these compounds, several MOs are shown to contribute to the conduction band of the crystal systems.[22–24] It has been recognized that the frontier orbitals for these compounds can be decomposed into several moieties, i.e., fragment MOs, and the electronic states have been analyzed using the microscopic tight-binding Hamiltonian based on the fragment MOs.[25]

The charge-transfer molecular compound (TTM-TTP)I_3 (Refs. 3 and 26–28) is now considered as another candidate of multi-molecular-orbital system.[29,30] In this compound, the non-magnetic insulating behavior at low temperature has been confirmed.[31–34] A charge ordering reflected by the alternation of valence of TTM-TTP molecule along the stacking direction has been proposed initially.[33,34] The experimental analysis based on Raman-scattering[35–37] and x-ray[38] measurements suggested a new type of charge-ordered state, "intra-molecular charge ordering (ICO)", which cannot be described by the conventional single-orbital approximation. By performing wavefunction-based *ab initio* calculations for the isolated ionic TTM-TTP molecule,[29] we previously revealed that this system has a multiconfigurational character.

In the present paper, we propose a scheme to build up an effective two-orbital extended Hubbard model for (TTM-TTP)I_3 and [Au(tmdt)$_2$], from *ab initio* multi-reference configuration-interaction (MR-CI) calculations.[39] To the best

of the authors' knowledge, this is the first analysis of parameter evaluations for multi-MO-based systems. The band structure in the so-called normal phase, i.e., no long-range-ordered state, is examined in terms of the evaluated tight-binding parameters. By noting that the resulting MOs exhibit bonding and anti-bonding character between the left and right moieties, we transform the two-orbital model into the fragment MO picture.

Some of the results have already been presented in Ref. 30, where the band structure for (TTM-TTP)I_3 turned out to be consistent with the direct band calculation based on the DFT results. Our goal in the present paper is to give an explicit derivation to extract model parameters in (TTM-TTP)I_3 and [Au(tmdt)$_2$] compounds. Indeed, one would like to unravel the origins of the ICO state in the former and the IAF state in the latter. The present paper is organized as follows. In section II, the characteristic feature of MOs is briefly reviewed. In section III, we derive the effective two-orbital Hubbard Hamiltonian for the isolated (TTM-TTP)$^+$ and [Au(tmdt)$_2$] molecules, and evaluate the parameters by using *ab initio* calculations. In section IV, the inter-molecular interactions are evaluated by focusing on two neighboring molecules in the crystal. In section V, we examine the band structure of the crystals. Section VI is devoted to the application to the fragment decomposition of MOs and examinations of its validity.

II. MOLECULAR ORBITALS

TTM-TTP stands for 2,5-bis[4,5-bis(methylthio)-1,3-dithiol-2-ylidene]-1,3,4,6-tetrathiapentalene and tmdt stands for trimethylenetetrathiafulvalenedithiolate. The molecular structures are shown in Fig. 1. The crystal structure of (TTM-TTP)I_3 is triclinic and the space group is $P\bar{1}$: the inversion center is located on the mid point of the TTM-TTP molecule. The formal charge of the TTM-TTP molecule is $+1$ due to the presence of mono-counterion I_3^-, and the HOMO is singly occupied, that is SOMO (singly-occupied-MO) in nature. For [Au(tmdt)$_2$], the crystal structure is also triclinic and the space group is $P\bar{1}$, where the inversion center is located on the metal center. Note that the isolated neutral molecule [Au(tmdt)$_2$] is a radical species. All our *ab initio* calculations were performed using the MOLCAS 7 package.[40] The atomic coordinates are read from the data of x-ray structure analysis.[19,26] Due to the presence of inversion center at the mid point of the molecules, the resulting MOs can be classified into gerade (g) or ungerade (u) with respect to the inversion center. The energy spectrum was calculated using a restricted open-shell Hartree-Fock (ROHF) procedure. Along these ROHF calculations, three electrons are likely to occupy the frontier g and u MOs. These MOs are likely to be singly occupied or doubly occupied in the ROHF calculations. In order to estimate the energies of the expected levels, we set the occupation numbers for both MOs as 1.5.[29] Under these conditions, for (TTM-TTP)$^+$, we obtain that the SOMO is u and HOMO-1 is g, in agreement with extended Hückel calculations,[4] and the resulting energy difference obtained from the ROHF calculation is ~ 0.4 eV.[29] For [Au(tmdt)$_2$], we obtain that the SOMO is g and HOMO-1 is u, in agreement with DFT-based *ab initio* calculations.[22] The notations for label of MOs are adopted to those in Ref. 22. The energy difference obtained from the ROHF calculation for isolated molecule is given by $(\varepsilon_{\rm SOMO}-\varepsilon_{\rm HOMO-1}) \simeq 0.26$ eV. Incidentally, the LUMO and the third-highest-occupied-molecular-orbital (HOMO-2) are sufficiently separated in energy, $(\varepsilon_{\rm LUMO}-\varepsilon_{\rm SOMO}) \simeq 6.07$ eV and $(\varepsilon_{\rm SOMO}-\varepsilon_{\rm HOMO-2}) \simeq 2.03$ eV.

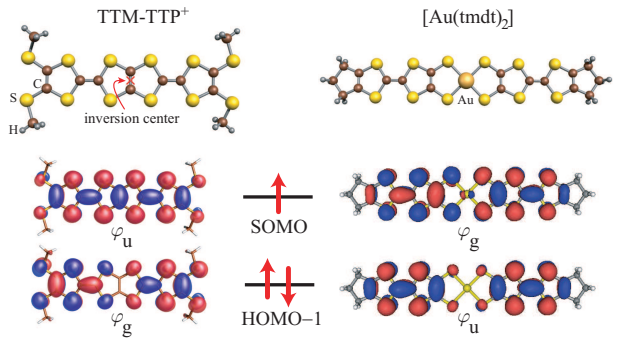

FIG. 1: The molecular structures and quasi-degenerate molecular orbitals for (TTM-TTP)$^+$ (left) and [Au(tmdt)$_2$] (right). For (TTM-TTP)$^+$, the singly-occupied-molecular-orbital (SOMO) has ungerade (u) symmetry with respect to the inversion center, while the second-highest-occupied-molecular-orbital (HOMO-1), has gerade (g) symmetry. For [Au(tmdt)$_2$], the inversion center is located on the metal (Au) center, and the SOMOs (HOMO-1) are of g (u) symmetries.

III. INTRA-MOLECULAR INTERACTIONS

We shall now focus on g and u MOs, shown in Fig. 1, and derive the effective two-orbital Hubbard Hamiltonian for the isolated TTM-TTP$^+$ and [Au(tmdt)$_2$] molecules. All the model parameters are determined so as to reproduce the energies of different electronic configurations obtained from the *ab initio* calculations.

A. Construction of the two-orbital Hubbard Hamiltonian

In this subsection, we derive the expression of the two-orbital tight-binding Hamiltonian for the isolated molecule. The relevant orbitals are written as $\varphi_{\rm g}(\boldsymbol{r})$ and $\varphi_{\rm u}(\boldsymbol{r})$, respectively. Due to the inversion symmetry around the midpoint of the molecule, the wavefunctions obey $\varphi_{\rm g}(\boldsymbol{r}) = \varphi_{\rm g}(-\boldsymbol{r})$ and $\varphi_{\rm u}(\boldsymbol{r}) = -\varphi_{\rm u}(-\boldsymbol{r})$, where the origin of the coordinate is taken as the inversion center (Fig. 1).

By focusing on the frontier orbitals, SOMO and HOMO-1, the full Hamiltonian for the isolated molecules is expressed as

$$H_{\text{1-mol}} = \sum_{\alpha}\sum_{\sigma} \bar{\varepsilon}^0_{\alpha} c^\dagger_{\alpha,\sigma} c_{\alpha,\sigma} + \frac{1}{2}\sum_{\alpha,\beta,\alpha',\beta'}\sum_{\sigma,\sigma'} (\alpha\alpha',\beta\beta')\, c^\dagger_{\alpha,\sigma} c_{\alpha',\sigma} c^\dagger_{\beta,\sigma'} c_{\beta',\sigma'}$$

$$+ \text{const.}, \tag{3.1}$$

where $c^\dagger_{\alpha,\sigma}$ stands for the creation operator of electron in MO $\alpha(=\text{g},\text{u})$ with spin $\sigma(=\uparrow,\downarrow)$. The orbital energies for the isolated molecules are represented by $\bar{\varepsilon}^0_\alpha$. For the electron-electron interactions, we adopt the notation for the integrals as

$$\begin{aligned}(\alpha\alpha',\beta\beta') &= \iint d\boldsymbol{r}_1 d\boldsymbol{r}_2 \\ &\times \varphi^*_\alpha(\boldsymbol{r}_1)\varphi_{\alpha'}(\boldsymbol{r}_1)\frac{1}{|\boldsymbol{r}_1-\boldsymbol{r}_2|}\varphi^*_\beta(\boldsymbol{r}_2)\varphi_{\beta'}(\boldsymbol{r}_2),\end{aligned} \tag{3.2}$$

where all the wavefunctions are real. Under the permutation of $\boldsymbol{r}_1$ and $\boldsymbol{r}_2$, we have the relations:

$$\begin{aligned}(\alpha\alpha',\beta\beta') &= (\beta\beta',\alpha\alpha') = (\alpha\alpha',\beta'\beta) \\ &= (\alpha'\alpha,\beta\beta') = (\alpha'\alpha,\beta'\beta).\end{aligned} \tag{3.3}$$

Due to the g/u symmetry of the MOs and relations (3.3), the number of independent interactions can be reduced. Depending on the choice of the indices $\alpha,\beta,\alpha',\beta'$ in Eq. (3.2), we can classify those integrals into intra- and inter-orbital interactions. The intra-orbital interactions $(\alpha\alpha,\alpha\alpha)$ represents the magnitude of interaction for electrons within the same MOs, in other words, the "on-site" Coulomb repulsions. Here we define the parameters:

$$U_\text{g} = (\text{gg},\text{gg}), \quad U_\text{u} = (\text{uu},\text{uu}). \tag{3.4}$$

For the inter-orbital case, the interactions involving odd number of ungerade MO, e.g., (gg,gu) vanishes due to the symmetry constraint. The possible interactions are $(\alpha\alpha,\beta\beta)$, $(\alpha\beta,\beta\alpha)$, and $(\alpha\beta,\alpha\beta)$ with $\alpha\neq\beta$, which correspond to the Coulomb integral, exchange integral, and pair-hopping interaction, respectively. We note that from Eq. (3.3), the amplitudes of the exchange integral and the pair-hopping interaction become identical $(\alpha\beta,\beta\alpha)=(\alpha\beta,\alpha\beta)$. We define the two-independent coupling constants given by

$$J_\text{H} = 2(\text{gu},\text{ug}) = 2(\text{gu},\text{gu}), \tag{3.5a}$$

$$U' = (\text{gg},\text{uu}) - \frac{1}{2}(\text{gu},\text{ug}), \tag{3.5b}$$

where J_H represents the Hund exchange coupling including the pair-hopping term, and U' is the inter-orbital Coulomb repulsion.

The level energies are determined by the eigenvalues of the ROHF. We note that the level energies $\bar{\epsilon}^0_\alpha$ in Eq. (3.1) do not correspond to the eigenvalues of ROHF, since the Hartree contributions arising from electron-electron interactions are not taken into account. These effects can be incorporated in terms of the model parameters U_g, U_u, and U', and we can re-define the MO level energies by

$$\varepsilon^0_\text{g} = \bar{\varepsilon}^0_\text{g} + U_\text{g}\langle c^\dagger_{\text{g},\uparrow}c_{\text{g},\uparrow}\rangle + U'\sum_\sigma\langle c^\dagger_{\text{u},\sigma}c_{\text{u},\sigma}\rangle, \tag{3.6a}$$

$$\varepsilon^0_\text{u} = \bar{\varepsilon}^0_\text{u} + U_\text{u}\langle c^\dagger_{\text{u},\uparrow}c_{\text{u},\uparrow}\rangle + U'\sum_\sigma\langle c^\dagger_{\text{g},\sigma}c_{\text{g},\sigma}\rangle, \tag{3.6b}$$

where the expectation values are determined by the Hartree-Fock calculation. Since the average charges on the each MO were set to $3/2$,[29] we obtain $\varepsilon^0_\text{g} = \bar{\varepsilon}^0_\text{g} + \frac{3}{4}U_\text{g} + \frac{3}{2}U'$ and $\varepsilon^0_\text{u} = \bar{\varepsilon}^0_\text{u} + \frac{3}{4}U_\text{u} + \frac{3}{2}U'$.

In order to express the Hamiltonian in a compact form, we introduce the density operators in the normal-ordered form:

$$n_{\text{g},\sigma} = c^\dagger_{\text{g},\sigma}c_{\text{g},\sigma} - \frac{3}{4}, \quad n_{\text{u},\sigma} = c^\dagger_{\text{u},\sigma}c_{\text{u},\sigma} - \frac{3}{4}, \tag{3.7}$$

and $n_\text{g} = (n_{\text{g},\uparrow}+n_{\text{g},\downarrow})$, $n_\text{u} = (n_{\text{u},\uparrow}+n_{\text{u},\downarrow})$. The Coulomb interactions having amplitudes U_g, U_u, and U' can be expressed in bilinear forms of these density operators. In terms of model parameters defined in Eqs. (3.4), (3.5), and (3.6), and also in terms of density operators given in Eq. (3.7), we obtain the effective two-orbital tight-binding Hamiltonian for the isolated molecules:

$$\begin{aligned}H_\text{1-mol} &= E_0 + \varepsilon^0_\text{g}n_\text{g} + \varepsilon^0_\text{u}n_\text{u} \\ &+ U_\text{g}n_{\text{g}\uparrow}n_{\text{g}\downarrow} + U_\text{u}n_{\text{u}\uparrow}n_{\text{u}\downarrow} + U'n_\text{g}n_\text{u} \\ &- J_\text{H}\left[\boldsymbol{S}_\text{g}\cdot\boldsymbol{S}_\text{u} - \frac{1}{2}(c^\dagger_{\text{g},\uparrow}c_{\text{u},\uparrow}c^\dagger_{\text{g},\downarrow}c_{\text{u},\downarrow} + \text{h.c.})\right],\end{aligned} \tag{3.8}$$

where $\boldsymbol{S}_\alpha$ is the spin operator given by $\boldsymbol{S}_\alpha = \frac{1}{2}\sum_{\sigma,\sigma'}c^\dagger_{\alpha,\sigma}\boldsymbol{\sigma}_{\sigma,\sigma'}c_{\alpha,\sigma'}$ with $\boldsymbol{\sigma}$ being the Pauli matrix. The energy constant E_0 and the level energy ε^0_g (ε^0_u) correspond to the total energy and the MO level energy for φ_g (φ_u), obtained by the ROHF calculations, respectively.

B. Possible configurations

In this subsection, we introduce the possible configurations for the two-orbital system including 0, 1, 2, 3, or 4 electrons. Let us stress that the MOs used to describe the different states remain unchanged and correspond to the three-electron case. For this purpose, we introduce the following notation:

$$\left|\begin{array}{c}\text{u}\\\hline\text{g}\end{array}\right\rangle. \tag{3.9}$$

The zero-electron state is given by

$$|\psi^{(0)}\rangle = \left|\begin{array}{c}-\\-\end{array}\right\rangle = |0\rangle, \tag{3.10a}$$

where $|0\rangle$ represents the Slater determinant in which the MOs are occupied up to the third-highest-occupied-MO.

For the one-electron states, we have two configurations

$$|\psi^{(1)}_\text{g}\rangle = \left|\begin{array}{c}-\\\uparrow\end{array}\right\rangle = c^\dagger_{\text{g},\uparrow}|0\rangle, \tag{3.10b}$$

$$|\psi^{(1)}_\text{u}\rangle = \left|\begin{array}{c}\uparrow\\-\end{array}\right\rangle = c^\dagger_{\text{u},\uparrow}|0\rangle. \tag{3.10c}$$

Since the same relations hold for the spin-down states, we focus only on the spin-up states hereafter.

For the two-electron states, there are four possible configurations, which can be classified depending on the symmetry and spin states. For the two-electron states with gerade symmetry, we have two configurations:

$$|\psi^{(2)}_{\mathrm{g,s},1}\rangle \;=\; \left|\begin{array}{c}-\\ \uparrow\downarrow\end{array}\right\rangle = c^\dagger_{\mathrm{g},\uparrow}c^\dagger_{\mathrm{g},\downarrow}|0\rangle, \tag{3.10d}$$

$$|\psi^{(2)}_{\mathrm{g,s},2}\rangle \;=\; \left|\begin{array}{c}\uparrow\downarrow\\ -\end{array}\right\rangle = c^\dagger_{\mathrm{u},\uparrow}c^\dagger_{\mathrm{u},\downarrow}|0\rangle, \tag{3.10e}$$

where both configurations are spin singlets. For the two-electron states with ungerade symmetry, there are also two configurations:

$$|\psi^{(2)}_{\mathrm{u,s}}\rangle \;=\; \left|\begin{array}{c}\downarrow\\ \uparrow\end{array}\right\rangle = \frac{1}{\sqrt{2}}(c^\dagger_{\mathrm{g},\uparrow}c^\dagger_{\mathrm{u},\downarrow} + c^\dagger_{\mathrm{u},\uparrow}c^\dagger_{\mathrm{g},\downarrow})|0\rangle, \tag{3.10f}$$

$$|\psi^{(2)}_{\mathrm{u,t}}\rangle \;=\; \left|\begin{array}{c}\uparrow\\ \uparrow\end{array}\right\rangle = c^\dagger_{\mathrm{g},\uparrow}c^\dagger_{\mathrm{u},\uparrow}|0\rangle, \tag{3.10g}$$

where the suffixes s and t represent the spin-singlet and spin-triplet states, respectively. The $S^z = 1$ component is only considered for the spin-triplet state.

The three-electron states are given by

$$|\psi^{(3)}_{\mathrm{g}}\rangle \;=\; \left|\begin{array}{c}\uparrow\downarrow\\ \uparrow\end{array}\right\rangle = c^\dagger_{\mathrm{g},\uparrow}c^\dagger_{\mathrm{u},\uparrow}c^\dagger_{\mathrm{u},\downarrow}|0\rangle, \tag{3.10h}$$

$$|\psi^{(3)}_{\mathrm{u}}\rangle \;=\; \left|\begin{array}{c}\uparrow\\ \uparrow\downarrow\end{array}\right\rangle = c^\dagger_{\mathrm{g},\uparrow}c^\dagger_{\mathrm{u},\uparrow}c^\dagger_{\mathrm{g},\downarrow}|0\rangle. \tag{3.10i}$$

Finally the four-electron state has a unique configuration:

$$|\psi^{(4)}\rangle \;=\; \left|\begin{array}{c}\uparrow\downarrow\\ \uparrow\downarrow\end{array}\right\rangle = c^\dagger_{\mathrm{g},\uparrow}c^\dagger_{\mathrm{u},\uparrow}c^\dagger_{\mathrm{g},\downarrow}c^\dagger_{\mathrm{u},\downarrow}|0\rangle. \tag{3.10j}$$

C. *Ab initio* calculations

The energies of the different configurations were evaluated by performing MR-CI calculations.[39] Several basis sets were used for convergence control, however, a weak dependence on the choice of basis set is observed. Throughout this paper, we adopt the basis sets contractions for the elements S(7s6p1d)/[4s3p1d], C(5s5p1d)/[3s2p1d], Au(13s10p9d6f)/[5s4p4d2f], and H(3s)/[1s]. The SOMO and HOMO-1 levels are well separated from the other MOs. Therefore, these two MOs are used to generate a so-called model space containing three electrons in two MOs. In order to evaluate full parameters, we also consider virtual states by removing/adding electrons.

We note that the two-electron gerade wavefunctions are given by the superpositions of the two configurations [Eqs. (3.10d) and (3.10e)]. By taking advantage of the information conveyed by the wavefunctions, we can access the Hamiltonian matrix expressed in the basis of Eqs. (3.10d) and (3.10e). Detailed formulation is given later (see Sec. IV C).

D. Parameter mapping

The model parameters in Eq. (3.8) can now be evaluated by relating the *ab initio* calculation results with the respective energies expressed in terms of the microscopic model parameters. From the Hamiltonian Eq. (3.8) and the configurations [Eq. (3.10)], the energy expectation for the zero-electron state $E^{(0)} = \langle\psi^{(0)}|H_{1\text{-mol}}|\psi^{(0)}\rangle$ can be expressed as

$$E^{(0)} = E_0 - \frac{3}{2}\varepsilon^0_{\mathrm{g}} - \frac{3}{2}\varepsilon^0_{\mathrm{u}} + \frac{9}{16}U_{\mathrm{g}} + \frac{9}{16}U_{\mathrm{u}} + \frac{9}{4}U'. \tag{3.11}$$

In the similar way, the respective energies $E^{(i)} = \langle\psi^{(i)}|H_{1\text{-mol}}|\psi^{(i)}\rangle$ can be expressed as

$$E^{(1)}_{\mathrm{g}} \;=\; E^{(0)} + \varepsilon^0_{\mathrm{g}} - \frac{3}{4}U_{\mathrm{g}} - \frac{3}{2}U', \tag{3.12a}$$

$$E^{(1)}_{\mathrm{u}} \;=\; E^{(0)} + \varepsilon^0_{\mathrm{u}} - \frac{3}{4}U_{\mathrm{u}} - \frac{3}{2}U', \tag{3.12b}$$

$$E^{(2)}_{\mathrm{g,s},1} \;=\; E^{(0)} + 2\varepsilon^0_{\mathrm{g}} - \frac{1}{2}U_{\mathrm{g}} - 3U', \tag{3.12c}$$

$$E^{(2)}_{\mathrm{g,s},2} \;=\; E^{(0)} + 2\varepsilon^0_{\mathrm{u}} - \frac{1}{2}U_{\mathrm{u}} - 3U', \tag{3.12d}$$

$$E^{(2)}_{\mathrm{u,s}} \;=\; E^{(0)} + \varepsilon^0_{\mathrm{g}} + \varepsilon^0_{\mathrm{u}} - \frac{3}{4}U_{\mathrm{g}} - \frac{3}{4}U_{\mathrm{u}} - 2U' + \frac{3}{4}J_{\mathrm{H}}, \tag{3.12e}$$

$$E^{(2)}_{\mathrm{u,t}} \;=\; E^{(0)} + \varepsilon^0_{\mathrm{g}} + \varepsilon^0_{\mathrm{u}} - \frac{3}{4}U_{\mathrm{g}} - \frac{3}{4}U_{\mathrm{u}} - 2U' - \frac{1}{4}J_{\mathrm{H}}, \tag{3.12f}$$

$$E^{(3)}_{\mathrm{g}} \;=\; E^{(0)} + \varepsilon^0_{\mathrm{g}} + 2\varepsilon^0_{\mathrm{u}} - \frac{3}{4}U_{\mathrm{g}} - \frac{1}{2}U_{\mathrm{u}} - \frac{5}{2}U', \tag{3.12g}$$

$$E^{(3)}_{\mathrm{u}} \;=\; E^{(0)} + 2\varepsilon^0_{\mathrm{g}} + \varepsilon^0_{\mathrm{u}} - \frac{1}{2}U_{\mathrm{g}} - \frac{3}{4}U_{\mathrm{u}} - \frac{5}{2}U', \tag{3.12h}$$

$$E^{(4)} \;=\; E^{(0)} + 2\varepsilon^0_{\mathrm{g}} + 2\varepsilon^0_{\mathrm{u}} - \frac{1}{2}U_{\mathrm{g}} - \frac{1}{2}U_{\mathrm{u}} - 2U'. \tag{3.12i}$$

Seven model parameters are to be determined, while ten energies are calculated for the respective configurations. Thus, the expressions for the model parameters in terms of *ab initio* energies are not expressed uniquely, but we can obtain the same numerical values irrespective of the expressions. One possible way to relate the configuration energies to the model parameters is given by

$$E_0 \;=\; -\frac{5}{16}E^{(0)} + \frac{3}{8}E^{(1)}_{\mathrm{g}} + \frac{3}{8}E^{(1)}_{\mathrm{u}} + \frac{9}{16}E^{(4)}, \tag{3.13a}$$

$$\varepsilon^0_{\mathrm{g}} \;=\; \frac{1}{8}E^{(0)} - \frac{1}{2}E^{(1)}_{\mathrm{g}} + \frac{3}{8}E^{(2)}_{\mathrm{g,s},1} - \frac{3}{8}E^{(2)}_{\mathrm{g,s},2} + \frac{3}{8}E^{(4)}, \tag{3.13b}$$

$$\varepsilon^0_{\mathrm{u}} \;=\; \frac{1}{8}E^{(0)} - \frac{1}{2}E^{(1)}_{\mathrm{u}}$$

$$-\frac{3}{8}E^{(2)}_{\mathrm{g,s},1}+\frac{3}{8}E^{(2)}_{\mathrm{g,s},2}+\frac{3}{8}E^{(4)}, \tag{3.13c}$$

$$U_{\mathrm{g}} = E^{(0)}-2E^{(1)}_{\mathrm{g}}+E^{(2)}_{\mathrm{g,s},1}, \tag{3.13d}$$

$$U_{\mathrm{u}} = E^{(0)}-2E^{(1)}_{\mathrm{u}}+E^{(2)}_{\mathrm{g,s},2}, \tag{3.13e}$$

$$U' = \frac{1}{4}E^{(0)}-\frac{1}{4}E^{(2)}_{\mathrm{g,s},1}-\frac{1}{4}E^{(2)}_{\mathrm{g,s},2}+\frac{1}{4}E^{(4)}, \tag{3.13f}$$

$$J_{\mathrm{H}} = E^{(2)}_{\mathrm{u,s}}-E^{(2)}_{\mathrm{u,t}}. \tag{3.13g}$$

We note that J_{H} can also be derived from the off-diagonal pair-hopping term $2\langle\psi^{(2)}_{\mathrm{g,s},1}|H|\psi^{(2)}_{\mathrm{g,s},2}\rangle$.

E. Results

The model parameters obtained in this way are summarized in Table I. The on-site Coulomb repulsions U_{g} and U_{u} are comparable to the values for the BEDT-TTF molecule ~ 4.2 eV.[6,7] We have also applied the present scheme to the TTF molecule and obtained large value of the "on-site" Coulomb interaction $\sim$ 6.2 eV. By comparing the values of U_{g} and U_{u} for TTM-TTP^{+}, we find a relatively smaller value for U_{g}, which can be explained by noting the left-right bonding character of the u MO while the g MO is anti-bonding, as seen in Fig. 1. On the other hand, the values of U_{g} and U_{u} for [Au(tmdt)$_2$] are almost degenerate as a consequence of the enhanced delocalization onto a larger system. The magnitudes of inter-orbital interactions, U' and J_{H}, are large compared with transition metal atom situations, satisfying $U_{\mathrm{atom}} = U'_{\mathrm{atom}} + J_{\mathrm{H\,atom}}$. In contrast with the transition metal atoms displaying a centrosymmetric potential, there is no constraint relation among the couplings, U_{g}, U_{u}, U', and J_{H}. Our results show that $(U_{\mathrm{g}}+U_{\mathrm{u}})/2 \approx 3 \sim 4$ eV and $(U'+J_{\mathrm{H}}) \approx 6$ eV. As a simplest and most intuitive example for the parameter evaluation of two-orbital system, we can consider the hydrogen molecule H_2 where the full CI calculations can be performed and we can get an insight into the large Hund coupling in molecular systems.[41]

TABLE I: Estimated parameters for the (TTM-TTP)$^{+}$ and [Au(tmdt)$_2$] molecules. All energies are in eV.

	TTM-TTP^{+}	[Au(tmdt)$_2$]
Level energy $\varepsilon^0_{\mathrm{g}}$	-8.63	-5.40
Level energy $\varepsilon^0_{\mathrm{u}}$	-8.21	-5.66
U_{g}	3.70	3.49
U_{u}	3.90	3.45
U'	2.82	2.48
J_{H}	3.19	3.65

IV. INTER-MOLECULAR INTERACTIONS

By extending the analysis of Sec. III, we evaluate the inter-molecular interactions by focusing on two neighboring molecules, i.e., dimer, in the crystal.

A. Construction of the two-orbital extended Hubbard Hamiltonian

A similar strategy can be applied to obtain the expression of the two-orbital Hamiltonian for the two-molecule dimer system. The molecule index is given by I and II. Each molecule has gerade and ungerade MOs reflecting the symmetry with respect to the each inversion center. For the gerade and ungerade MOs on molecule I, we adopt the notations $\varphi_{\mathrm{g,I}}$ and $\varphi_{\mathrm{u,I}}$, respectively ($\varphi_{\mathrm{g,II}}$ and $\varphi_{\mathrm{u,II}}$ for molecule II). The MOs correspond to the strictly non-interacting situation. Practically, they were determined by pulling apart the two molecules. The respective MOs are shown in Fig. 2. The inversion transformations with respect to the inversion centers located on the molecule ($\boldsymbol{R}_{\mathrm{I}}$ and $\boldsymbol{R}_{\mathrm{II}}$) are represented as, e.g., $\varphi_{\mathrm{g,I}}(\boldsymbol{R}_{\mathrm{I}}+\boldsymbol{r}) = \varphi_{\mathrm{g,I}}(\boldsymbol{R}_{\mathrm{I}}-\boldsymbol{r})$ and $\varphi_{\mathrm{u,I}}(\boldsymbol{R}_{\mathrm{I}}+\boldsymbol{r}) = -\varphi_{\mathrm{u,I}}(\boldsymbol{R}_{\mathrm{I}}-\boldsymbol{r})$. From the x-ray structure analysis, it has been shown that the system exhibits another inversion center located at midpoint between two molecules.[19,26] For the inversion transformation around the midpoint, the wavefunctions of the two molecules follow the relations

$$\varphi_{\mathrm{g,I}}(\boldsymbol{r}) = \varphi_{\mathrm{g,II}}(-\boldsymbol{r}), \quad \varphi_{\mathrm{u,I}}(\boldsymbol{r}) = -\varphi_{\mathrm{u,II}}(-\boldsymbol{r}). \tag{4.1}$$

The $\varphi_{\mathrm{g,I}}$, $\varphi_{\mathrm{u,I}}$, $\varphi_{\mathrm{g,II}}$, and $\varphi_{\mathrm{u,II}}$ MOs are used to define the model space.

For the inter-molecular interactions, the most important parameters are transfer integrals between the molecules. We de-

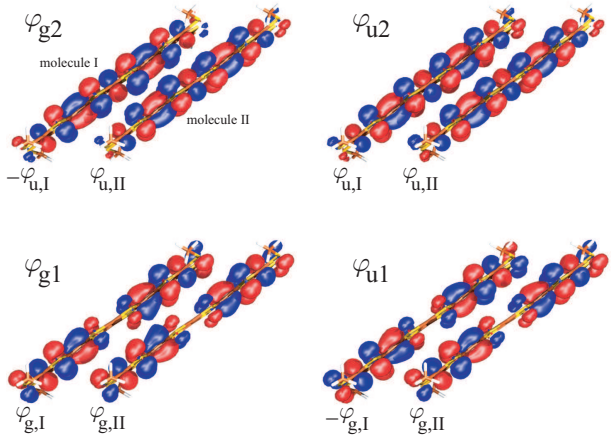

FIG. 2: Side view of the "effective molecular orbitals" for the two-molecule dimer system. The MOs of each TTM-TTP molecule are the same as those calculated for the isolated molecule. The wavefunctions φ_{g1} and φ_{u1} (φ_{g2} and φ_{u2}) are given by the linear combinations of two g (u) MOs obtained from the isolated-molecule calculations.

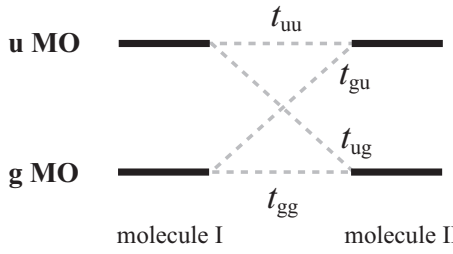

FIG. 3: Tight-binding parameters for the two-molecule dimer system. We note $t_{\rm gu} = -t_{\rm ug}$ due to the presence of inversion center between two molecules.

fine such transfer integrals ($\alpha, \beta =$ g or u) as:

$$\begin{aligned} t_{\alpha\beta} &= -\langle \alpha_{\rm I}|H|\beta_{\rm II}\rangle \\ &= -\int d\boldsymbol{r}\, \varphi^*_{\alpha,{\rm I}}(\boldsymbol{r})\, H\, \varphi_{\beta,{\rm II}}(\boldsymbol{r}). \end{aligned} \tag{4.2}$$

In the two-orbital system, four kinds of transfer integral are possible (Fig. 3), which are explicitly given by

$$t_{\rm gg} = -\langle {\rm g_I}|H|{\rm g_{II}}\rangle, \tag{4.3a}$$

$$t_{\rm uu} = -\langle {\rm u_I}|H|{\rm u_{II}}\rangle, \tag{4.3b}$$

$$t_{\rm gu} = -\langle {\rm g_I}|H|{\rm u_{II}}\rangle, \tag{4.3c}$$

$$t_{\rm ug} = -\langle {\rm u_I}|H|{\rm g_{II}}\rangle. \tag{4.3d}$$

The Hermitian condition indicates $\langle \alpha_{\rm I}|H|\beta_{\rm II}\rangle = \langle \beta_{\rm II}|H|\alpha_{\rm I}\rangle$. By applying the inversion transformation given by Eq. (4.1), we find $t_{\rm gu} = -t_{\rm ug}$.

In addition to the transfer integrals between the molecules, we have an extra one-electron interaction term in the two-molecule system. If one picks up two molecules from the crystal, the inversion center within each molecule is lost and the mixtures of MOs, i.e., $\langle {\rm g_I}|H|{\rm u_I}\rangle$ and $\langle {\rm g_{II}}|H|{\rm u_{II}}\rangle$ become non-zero. Such a symmetry-breaking interaction is given by

$$H'_\Delta = \Delta\varepsilon_{\rm gu} \sum_\sigma (c^\dagger_{{\rm g,I},\sigma} c_{{\rm u,I},\sigma} - c^\dagger_{{\rm g,II},\sigma} c_{{\rm u,II},\sigma} + {\rm h.c.}). \tag{4.4}$$

In terms of the *ab initio* Hamiltonian H, this coupling constant accounting for this symmetry-breaking interaction would be represented as $\Delta\varepsilon_{\rm gu} = \frac{1}{2}\langle {\rm g_I}|H|{\rm u_I}\rangle - \frac{1}{2}\langle {\rm g_{II}}|H|{\rm u_{II}}\rangle$. In the crystal, such interaction disappears due to the periodicity of the interactions.

In analogy with Eq. (3.1), the electron-electron interaction terms are expressed as

$$\begin{aligned} (\alpha_i\alpha'_{i'}, \beta_j\beta'_{j'}) &= \iint d\boldsymbol{r}_1 d\boldsymbol{r}_2 \\ &\times \varphi^*_{\alpha,i}(\boldsymbol{r}_1)\varphi_{\alpha',i'}(\boldsymbol{r}_1)\frac{1}{|\boldsymbol{r}_1 - \boldsymbol{r}_2|}\varphi^*_{\beta,j}(\boldsymbol{r}_2)\varphi_{\beta',j'}(\boldsymbol{r}_2), \end{aligned} \tag{4.5}$$

where $\alpha, \beta =$ g or u, and the molecule index is given by $i, j, i', j' (=$ I or II$)$. We assume that all the wavefunctions are real and the relation of Eq. (3.3) still holds in the present case. Under the inversion transformation ($\boldsymbol{r} \to -\boldsymbol{r}$) given by Eq. (4.1), we find several relations, e.g., $({\rm g_I u_I}, {\rm u_I u_I}) = -({\rm g_{II} u_{II}}, {\rm u_{II} u_{II}})$. Since the MOs are localized on each molecule, we find that the "two-center" integrals given by, e.g., $(\alpha_{\rm I}\alpha'_{\rm II}, \beta_{\rm II}\beta'_{\rm I})$ and $(\alpha_{\rm I}\alpha'_{\rm I}, \beta_{\rm I}\beta'_{\rm II})$ are negligibly small due to small overlaps and cannot be determined within the numerical error. The interactions expressed as $(\alpha_{\rm I}\alpha'_{\rm I}, \beta_{\rm I}\beta'_{\rm I})$, $(\alpha_{\rm II}\alpha'_{\rm II}, \beta_{\rm II}\beta'_{\rm II})$, $(\alpha_{\rm I}\alpha'_{\rm I}, \beta_{\rm II}\beta'_{\rm II})$, and $(\alpha_{\rm II}\alpha'_{\rm II}, \beta_{\rm I}\beta'_{\rm I})$ are the only relevant interactions. We also note here that the hopping parameters, Eq. (4.2), have been defined in the one-electron picture and some of two-electron integrals, e.g., $({\rm g_I g_I}, {\rm u_I u_{II}})$ and $({\rm g_I u_I}, {\rm u_I u_{II}})$, can contribute to them in the present two-orbital systems. However, these contributions are small two-center integrals and thus the simple definition of the transfer integrals can be justified. Depending on the choice of indices $\alpha, \alpha', \beta, \beta'$ and i, i', j, j', the interactions (4.5) can be classified into five categories: (i) all the indices are identical, (ii) three-indices are identical, (iii) two pairs of identical indices, (iv) all indices are different, and (v) one pair of identical indices. We here examine each case separately.

(i) The interactions are nothing but the local on-site Coulomb interactions, given by $U_{\rm g} = ({\rm g_I g_I}, {\rm g_I g_I}) = ({\rm g_{II} g_{II}}, {\rm g_{II} g_{II}})$ and $U_{\rm u} = ({\rm u_I u_I}, {\rm u_I u_I}) = ({\rm u_{II} u_{II}}, {\rm u_{II} u_{II}})$, which are the same relations as Eq. (3.4).

(ii) The possible interactions are $({\rm g_I g_I}, {\rm g_I u_I})$, $({\rm u_I u_I}, {\rm u_I g_I})$, and the interactions with the molecular index I and II interchanged. These couplings vanish due to the inversion transformation within each molecule.

(iii) In addition to the intra-molecular interactions $J_{\rm H}$ and U', we introduce the couplings: $V_{\rm gg} = ({\rm g_I g_I}, {\rm g_{II} g_{II}})$, $V_{\rm uu} = ({\rm u_I u_I}, {\rm u_{II} u_{II}})$, $V_{\rm gu} = ({\rm g_I g_I}, {\rm u_{II} u_{II}})$, and $V_{\rm ug} = ({\rm u_I u_I}, {\rm g_{II} g_{II}})$, where $V_{\rm gu} = V_{\rm ug}$. These represent the "inter-site" Coulomb repulsions.

(iv) In this category, the only relevant parameter is given by

$$\begin{aligned} I &= ({\rm g_I u_I}, {\rm g_{II} u_{II}}) = ({\rm g_I u_I}, {\rm u_{II} g_{II}}) \\ &= ({\rm u_I g_I}, {\rm u_{II} g_{II}}) = ({\rm u_I g_I}, {\rm g_{II} u_{II}}). \end{aligned} \tag{4.6}$$

This term can be regarded as an "orbital exchange" between neighboring molecules.

(v) In this category, we have only two independent parameters, given by

$$\begin{aligned} X_{\rm g} &= ({\rm g_I g_I}, {\rm g_{II} u_{II}}) = ({\rm g_I g_I}, {\rm u_{II} g_{II}}) \\ &= -({\rm g_{II} g_{II}}, {\rm g_I u_I}) = -({\rm g_{II} g_{II}}, {\rm u_I g_I}), \end{aligned} \tag{4.7a}$$

$$\begin{aligned} X_{\rm u} &= ({\rm u_I u_I}, {\rm g_{II} u_{II}}) = ({\rm u_I u_I}, {\rm u_{II} g_{II}}) \\ &= -({\rm u_{II} u_{II}}, {\rm g_I u_I}) = -({\rm u_{II} u_{II}}, {\rm u_I g_I}). \end{aligned} \tag{4.7b}$$

As in the case of the isolated molecule, we introduce the density operators in the normal-ordered form: $n_{{\rm g},i,\sigma} = (c^\dagger_{{\rm g},i,\sigma} c_{{\rm g},i,\sigma} - \frac{3}{4})$ and $n_{{\rm u},i,\sigma} = (c^\dagger_{{\rm u},i,\sigma} c_{{\rm u},i,\sigma} - \frac{3}{4})$ where $i = {\rm I}, {\rm II}$. Thus, in terms of model parameters, the full extended Hubbard Hamiltonian for the two-molecule system is

expressed as

$$
\begin{aligned}
H_{2\text{-mol}} \;=\; & \sum_{j=\mathrm{I},\mathrm{II}} H_{1\text{-mol}} + \sum_{j=\mathrm{I},\mathrm{II}} \left(\Delta\varepsilon_{\mathrm{g}} n_{\mathrm{g},j} + \Delta\varepsilon_{\mathrm{u}} n_{\mathrm{u},j}\right) \\
& - t_{\mathrm{gg}} \sum_{\sigma} (c^{\dagger}_{\mathrm{g,I},\sigma} c_{\mathrm{g,II},\sigma} + \mathrm{h.c.}) \\
& - t_{\mathrm{uu}} \sum_{\sigma} (c^{\dagger}_{\mathrm{u,I},\sigma} c_{\mathrm{u,II},\sigma} + \mathrm{h.c.}) \\
& - t_{\mathrm{gu}} \sum_{\sigma} (c^{\dagger}_{\mathrm{g,I},\sigma} c_{\mathrm{u,II},\sigma} - c^{\dagger}_{\mathrm{u,I},\sigma} c_{\mathrm{g,II},\sigma} + \mathrm{h.c.}) \\
& + V_{\mathrm{gg}} n_{\mathrm{g,I}} n_{\mathrm{g,II}} + V_{\mathrm{uu}} n_{\mathrm{u,I}} n_{\mathrm{u,II}} \\
& + V_{\mathrm{gu}} \left(n_{\mathrm{g,I}} n_{\mathrm{u,II}} + n_{\mathrm{u,I}} n_{\mathrm{g,II}}\right) \\
& + I \sum_{\sigma,\sigma'} \Big(c^{\dagger}_{\mathrm{g,I},\sigma} c_{\mathrm{u,I},\sigma} c^{\dagger}_{\mathrm{g,II},\sigma'} c_{\mathrm{u,II},\sigma'} \\
& \qquad + c^{\dagger}_{\mathrm{g,I},\sigma} c_{\mathrm{u,I},\sigma} c^{\dagger}_{\mathrm{u,II},\sigma'} c_{\mathrm{g,II},\sigma'} + \mathrm{h.c.} \Big) \\
& + X_{\mathrm{g}} \sum_{\sigma} \Big[n_{\mathrm{g,I}} (c^{\dagger}_{\mathrm{g,II},\sigma} c_{\mathrm{u,II},\sigma} + \mathrm{h.c.}) - (\mathrm{I} \leftrightarrow \mathrm{II}) \Big] \\
& + X_{\mathrm{u}} \sum_{\sigma} \Big[n_{\mathrm{u,I}} (c^{\dagger}_{\mathrm{g,II},\sigma} c_{\mathrm{u,II},\sigma} + \mathrm{h.c.}) - (\mathrm{I} \leftrightarrow \mathrm{II}) \Big] \\
& + H'_{\Delta} + \Delta E_0, \qquad (4.8)
\end{aligned}
$$

where $H_{1\text{-mol}}$ is the Hamiltonian for the isolated molecule given in Eq. (3.8). The $\Delta\varepsilon_{\mathrm{g}}$ and $\Delta\varepsilon_{\mathrm{u}}$ terms represent the energy-level shift due to the neighboring molecules, i.e., so-called crystal-field effect. These terms also include the Hartree contributions arising from the intermolecular density-density interactions, V_{gg}, V_{uu}, and V_{gu}, as in the isolated molecule [Eq. (3.6)]. The Hartree contributions from the X_{g} and X_{u} interactions can be included into the H'_{Δ} term [Eq. (4.4)]. The term ΔE_0 represents the constant energy shift.

B. Possible configurations

For the two-molecule systems, four MOs must be considered. Due to the presence of the transfer integrals between the molecules, the wavefunctions for the two-molecule system are given by the linear combinations of MOs for the isolated molecules. The fragment MOs which exhibit g and u characters within each molecule, namely $(\varphi_{\mathrm{g,I}}, \varphi_{\mathrm{u,I}})$ and $(\varphi_{\mathrm{g,II}}, \varphi_{\mathrm{u,II}})$, were used to build the symmetry-adapted MOs, given by

$$\varphi_{\mathrm{g1}} = \frac{1}{\sqrt{2}}(\varphi_{\mathrm{g,I}} + \varphi_{\mathrm{g,II}}), \qquad (4.9a)$$

$$\varphi_{\mathrm{u1}} = \frac{1}{\sqrt{2}}(-\varphi_{\mathrm{g,I}} + \varphi_{\mathrm{g,II}}), \qquad (4.9b)$$

$$\varphi_{\mathrm{g2}} = \frac{1}{\sqrt{2}}(-\varphi_{\mathrm{u,I}} + \varphi_{\mathrm{u,II}}), \qquad (4.9c)$$

$$\varphi_{\mathrm{u2}} = \frac{1}{\sqrt{2}}(\varphi_{\mathrm{u,I}} + \varphi_{\mathrm{u,II}}), \qquad (4.9d)$$

and drawn in Fig. 2.

As in the case of the isolated molecule system, different configurations were considered. In order to specify each configuration on the new MO basis [Eq. (4.9)], we introduce the following:

$$\left| \begin{array}{cc} \underline{\mathrm{g}_2} & \underline{\mathrm{u}_2} \\ \underline{\mathrm{g}_1} & \underline{\mathrm{u}_1} \end{array} \right\rangle . \qquad (4.10)$$

In the two-molecule systems $[(\mathrm{TTM\text{-}TTP})^{-}]_2$ and $[\mathrm{Au(tmdt)_2}]_2$, six electrons are likely to occupy these four MOs. In order to estimate the magnitudes of the Coulomb interactions, we have to add/remove electrons from the six-electron ground state. In the present analysis, we consider all the configurations with $n = 0$, 1, and 2 electrons. The extensions to the states with $n \geq 3$ are straightforward. However, we will see that the information is sufficient to evaluate the model parameters.

The zero-electron state is given by

$$|\psi^{(0)}\rangle = \left| \begin{array}{cc} - & - \\ - & - \end{array} \right\rangle = |0\rangle, \qquad (4.11)$$

while the one-electron states are

$$|\psi^{(1)}_{\mathrm{g},1}\rangle = \left| \begin{array}{cc} - & - \\ \uparrow & - \end{array} \right\rangle = c^{\dagger}_{\mathrm{g}_1,\uparrow}|0\rangle, \qquad (4.12a)$$

$$|\psi^{(1)}_{\mathrm{g},2}\rangle = \left| \begin{array}{cc} \uparrow & - \\ - & - \end{array} \right\rangle = c^{\dagger}_{\mathrm{g}_2,\uparrow}|0\rangle, \qquad (4.12b)$$

$$|\psi^{(1)}_{\mathrm{u},1}\rangle = \left| \begin{array}{cc} - & - \\ - & \uparrow \end{array} \right\rangle = c^{\dagger}_{\mathrm{u}_1,\uparrow}|0\rangle, \qquad (4.12c)$$

$$|\psi^{(1)}_{\mathrm{u},2}\rangle = \left| \begin{array}{cc} - & \uparrow \\ - & - \end{array} \right\rangle = c^{\dagger}_{\mathrm{u}_2,\uparrow}|0\rangle, \qquad (4.12d)$$

where $c_{\mathrm{g}_1,\sigma}$ $c_{\mathrm{u}_1,\sigma}$, $c_{\mathrm{g}_2,\sigma}$, and $c_{\mathrm{u}_2,\sigma}$ represent the annihilation operators corresponding to the wavefunctions, φ_{g1}, φ_{u1}, φ_{g2}, and φ_{u2}, respectively, given in Fig. 2 and Eq. (4.9).

We also consider all the two-electron configurations. All the resulting states are listed in Table II, depending on the g/u and singlet/triplet natures.

C. *Ab initio* calculations for the two-molecule dimer systems

The molecule pairs which we consider are extracted from the x-ray data, and are shown in Fig. 4. In the case of [001] two-TTM-TTP-molecule pair, the "molecular orbitals" obtained from the ROHF calculation are given in Fig. 2. The assumption that we made here is that the MOs obtained in the isolated-molecule calculation are similar to the MOs in crystal.

MR-CI calculations were performed to extract full parameters by taking advantage of the wavefunction information. In this scheme, one can access the off-diagonal elements of the

TABLE II: Possible configurations for the two-electron states in the two-molecule dimer systems, the corresponding expressions in the molecular index I and II, and the energy expectation values represented in terms of the parameters in the extended Hubbard Hamiltonian $E_\nu^{(2)} = \langle\psi_\nu^{(2)}|H_{2\text{-mol}}|\psi_\nu^{(2)}\rangle$, where $E^{(2)} = E^{(0)} + \varepsilon_{\rm g} + \varepsilon_{\rm u} - 3(U_{\rm g} + U_{\rm u})/4 - 5U'/2 - 3(V_{\rm gg} + V_{\rm uu})/2 - 5V_{\rm gu}/2$. The suffix s and t represent the spin-singlet and spin-triplet states, respectively.

	Configurations		Representation on the molecular-based fragment MOs	Energy expectation values
Gerade, singlet	$\lvert\psi^{(2)}_{\rm g,s,1}\rangle =$	$\left\lvert \begin{matrix} - & - \\ \uparrow\downarrow & - \end{matrix} \right\rangle$	$\frac{1}{2}\left(\lvert {\rm g_I}\bar{\rm g_I}\rangle + \lvert {\rm g_{II}}\bar{\rm g_{II}}\rangle + \lvert {\rm g_I}\bar{\rm g_{II}}\rangle + \lvert {\rm g_{II}}\bar{\rm g_I}\rangle\right)$	$E^{(2)} + \varepsilon_{\rm g} - \varepsilon_{\rm u} - \frac{1}{4}U_{\rm g} + \frac{3}{4}U_{\rm u} - \frac{1}{2}U'$ $-V_{\rm gg} + \frac{3}{2}V_{\rm uu} - \frac{1}{2}V_{\rm gu} - 2t_{\rm gg}$
	$\lvert\psi^{(2)}_{\rm g,s,2}\rangle =$	$\left\lvert \begin{matrix} \downarrow & - \\ \uparrow & - \end{matrix} \right\rangle$	$-\frac{1}{2\sqrt{2}}\left(\lvert {\rm g_I}\bar{\rm u_I}\rangle + \lvert {\rm u_I}\bar{\rm g_I}\rangle - \lvert {\rm g_{II}}\bar{\rm u_{II}}\rangle - \lvert {\rm u_{II}}\bar{\rm g_{II}}\rangle\right)$ $+\frac{1}{2\sqrt{2}}\left(\lvert {\rm g_I}\bar{\rm u_{II}}\rangle + \lvert {\rm u_{II}}\bar{\rm g_I}\rangle - \lvert {\rm g_{II}}\bar{\rm u_I}\rangle - \lvert {\rm u_I}\bar{\rm g_{II}}\rangle\right)$	$E^{(2)} + \frac{3}{8}J_{\rm H} - \frac{1}{2}I + (t_{\rm uu} - t_{\rm gg})$
	$\lvert\psi^{(2)}_{\rm g,s,3}\rangle =$	$\left\lvert \begin{matrix} \uparrow\downarrow & - \\ - & - \end{matrix} \right\rangle$	$\frac{1}{2}\left(\lvert {\rm u_I}\bar{\rm u_I}\rangle + \lvert {\rm u_{II}}\bar{\rm u_{II}}\rangle - \lvert {\rm u_I}\bar{\rm u_{II}}\rangle - \lvert {\rm u_{II}}\bar{\rm u_I}\rangle\right)$	$E^{(2)} - \varepsilon_{\rm g} + \varepsilon_{\rm u} + \frac{3}{4}U_{\rm g} - \frac{1}{4}U_{\rm u} - \frac{1}{2}U'$ $+\frac{3}{2}V_{\rm gg} - V_{\rm uu} - \frac{1}{2}V_{\rm gu} + 2t_{\rm uu}$
	$\lvert\psi^{(2)}_{\rm g,s,4}\rangle =$	$\left\lvert \begin{matrix} - & - \\ - & \uparrow\downarrow \end{matrix} \right\rangle$	$\frac{1}{2}\left(\lvert {\rm g_I}\bar{\rm g_I}\rangle + \lvert {\rm g_{II}}\bar{\rm g_{II}}\rangle - \lvert {\rm g_I}\bar{\rm g_{II}}\rangle - \lvert {\rm g_{II}}\bar{\rm g_I}\rangle\right)$	$E^{(2)} + \varepsilon_{\rm g} - \varepsilon_{\rm u} - \frac{1}{4}U_{\rm g} + \frac{3}{4}U_{\rm u} - \frac{1}{2}U'$ $-V_{\rm gg} + \frac{3}{2}V_{\rm uu} - \frac{1}{2}V_{\rm gu} + 2t_{\rm gg}$
	$\lvert\psi^{(2)}_{\rm g,s,5}\rangle =$	$\left\lvert \begin{matrix} - & \downarrow \\ - & \uparrow \end{matrix} \right\rangle$	$-\frac{1}{2\sqrt{2}}\left(\lvert {\rm g_I}\bar{\rm u_I}\rangle + \lvert {\rm u_I}\bar{\rm g_I}\rangle - \lvert {\rm g_{II}}\bar{\rm u_{II}}\rangle - \lvert {\rm u_{II}}\bar{\rm g_{II}}\rangle\right)$ $-\frac{1}{2\sqrt{2}}\left(\lvert {\rm g_I}\bar{\rm u_{II}}\rangle + \lvert {\rm u_{II}}\bar{\rm g_I}\rangle - \lvert {\rm g_{II}}\bar{\rm u_I}\rangle - \lvert {\rm u_I}\bar{\rm g_{II}}\rangle\right)$	$E^{(2)} + \frac{3}{8}J_{\rm H} - \frac{1}{2}I - (t_{\rm uu} - t_{\rm gg})$
	$\lvert\psi^{(2)}_{\rm g,s,6}\rangle =$	$\left\lvert \begin{matrix} - & \uparrow\downarrow \\ - & - \end{matrix} \right\rangle$	$\frac{1}{2}\left(\lvert {\rm u_I}\bar{\rm u_I}\rangle + \lvert {\rm u_{II}}\bar{\rm u_{II}}\rangle + \lvert {\rm u_I}\bar{\rm u_{II}}\rangle + \lvert {\rm u_{II}}\bar{\rm u_I}\rangle\right)$	$E^{(2)} - \varepsilon_{\rm g} + \varepsilon_{\rm u} + \frac{3}{4}U_{\rm g} - \frac{1}{4}U_{\rm u} - \frac{1}{2}U'$ $+\frac{3}{2}V_{\rm gg} - V_{\rm uu} - \frac{1}{2}V_{\rm gu} - 2t_{\rm uu}$
Gerade, triplet	$\lvert\psi^{(2)}_{\rm g,t,1}\rangle =$	$\left\lvert \begin{matrix} \uparrow & - \\ \uparrow & - \end{matrix} \right\rangle$	$-\frac{1}{2}\left(\lvert {\rm g_I}{\rm u_I}\rangle - \lvert {\rm g_{II}}{\rm u_{II}}\rangle - \lvert {\rm g_I}{\rm u_{II}}\rangle + \lvert {\rm g_{II}}{\rm u_I}\rangle\right)$	$E^{(2)} - \frac{1}{8}J_{\rm H} + \frac{1}{2}I + (t_{\rm uu} - t_{\rm gg})$
	$\lvert\psi^{(2)}_{\rm g,t,2}\rangle =$	$\left\lvert \begin{matrix} - & \uparrow \\ - & \uparrow \end{matrix} \right\rangle$	$-\frac{1}{2}\left(\lvert {\rm g_I}{\rm u_I}\rangle - \lvert {\rm g_{II}}{\rm u_{II}}\rangle + \lvert {\rm g_I}{\rm u_{II}}\rangle - \lvert {\rm g_{II}}{\rm u_I}\rangle\right)$	$E^{(2)} - \frac{1}{8}J_{\rm H} + \frac{1}{2}I - (t_{\rm uu} - t_{\rm gg})$
Ungerade, singlet	$\lvert\psi^{(2)}_{\rm u,s,1}\rangle =$	$\left\lvert \begin{matrix} - & - \\ \uparrow & \downarrow \end{matrix} \right\rangle$	$-\frac{1}{\sqrt{2}}\left(\lvert {\rm g_I}\bar{\rm g_I}\rangle - \lvert {\rm g_{II}}\bar{\rm g_{II}}\rangle\right)$	$E^{(2)} + \varepsilon_{\rm g} - \varepsilon_{\rm u} + \frac{1}{4}U_{\rm g} + \frac{3}{4}U_{\rm u} - \frac{1}{2}U'$ $-\frac{3}{2}V_{\rm gg} + \frac{3}{2}V_{\rm uu} - \frac{1}{2}V_{\rm gu}$
	$\lvert\psi^{(2)}_{\rm u,s,2}\rangle =$	$\left\lvert \begin{matrix} - & \downarrow \\ \uparrow & - \end{matrix} \right\rangle$	$\frac{1}{2\sqrt{2}}\left(\lvert {\rm g_I}\bar{\rm u_I}\rangle + \lvert {\rm u_I}\bar{\rm g_I}\rangle + \lvert {\rm g_{II}}\bar{\rm u_{II}}\rangle + \lvert {\rm u_{II}}\bar{\rm g_{II}}\rangle\right)$ $+\frac{1}{2\sqrt{2}}\left(\lvert {\rm g_I}\bar{\rm u_{II}}\rangle + \lvert {\rm u_{II}}\bar{\rm g_I}\rangle + \lvert {\rm g_{II}}\bar{\rm u_I}\rangle + \lvert {\rm u_I}\bar{\rm g_{II}}\rangle\right)$	$E^{(2)} + \frac{3}{8}J_{\rm H} + \frac{1}{2}I - (t_{\rm uu} + t_{\rm gg})$
	$\lvert\psi^{(2)}_{\rm u,s,3}\rangle =$	$\left\lvert \begin{matrix} \uparrow & - \\ - & \downarrow \end{matrix} \right\rangle$	$\frac{1}{2\sqrt{2}}\left(\lvert {\rm g_I}\bar{\rm u_I}\rangle + \lvert {\rm u_I}\bar{\rm g_I}\rangle + \lvert {\rm g_{II}}\bar{\rm u_{II}}\rangle + \lvert {\rm u_{II}}\bar{\rm g_{II}}\rangle\right)$ $-\frac{1}{2\sqrt{2}}\left(\lvert {\rm g_I}\bar{\rm u_{II}}\rangle + \lvert {\rm u_{II}}\bar{\rm g_I}\rangle + \lvert {\rm g_{II}}\bar{\rm u_I}\rangle + \lvert {\rm u_I}\bar{\rm g_{II}}\rangle\right)$	$E^{(2)} + \frac{3}{8}J_{\rm H} + \frac{1}{2}I + (t_{\rm uu} + t_{\rm gg})$
	$\lvert\psi^{(2)}_{\rm u,s,4}\rangle =$	$\left\lvert \begin{matrix} \uparrow & \downarrow \\ - & - \end{matrix} \right\rangle$	$-\frac{1}{\sqrt{2}}\left(\lvert {\rm u_I}\bar{\rm u_I}\rangle - \lvert {\rm u_{II}}\bar{\rm u_{II}}\rangle\right)$	$E^{(2)} - \varepsilon_{\rm g} + \varepsilon_{\rm u} + \frac{3}{4}U_{\rm g} + \frac{1}{4}U_{\rm u}$ $-\frac{1}{2}U' + \frac{3}{2}V_{\rm gg} - \frac{3}{2}V_{\rm uu} - \frac{1}{2}V_{\rm gu}$
Ungerade, triplet	$\lvert\psi^{(2)}_{\rm u,t,1}\rangle =$	$\left\lvert \begin{matrix} - & - \\ \uparrow & \uparrow \end{matrix} \right\rangle$	$\lvert {\rm g_I}{\rm g_{II}}\rangle$	$E^{(2)} + \varepsilon_{\rm g} - \varepsilon_{\rm u} - \frac{3}{4}U_{\rm g} + \frac{3}{4}U_{\rm u}$ $-\frac{1}{2}U' - \frac{1}{2}V_{\rm gg} + \frac{3}{2}V_{\rm uu} - \frac{1}{2}V_{\rm gu}$
	$\lvert\psi^{(2)}_{\rm u,t,2}\rangle =$	$\left\lvert \begin{matrix} - & \uparrow \\ \uparrow & - \end{matrix} \right\rangle$	$\frac{1}{2}\left(\lvert {\rm g_I}{\rm u_I}\rangle + \lvert {\rm g_{II}}{\rm u_{II}}\rangle + \lvert {\rm g_I}{\rm u_{II}}\rangle - \lvert {\rm u_I}{\rm g_{II}}\rangle\right)$	$E^{(2)} - \frac{1}{8}J_{\rm H} - \frac{1}{2}I - (t_{\rm uu} + t_{\rm gg})$
	$\lvert\psi^{(2)}_{\rm u,t,3}\rangle =$	$\left\lvert \begin{matrix} \uparrow & - \\ - & \uparrow \end{matrix} \right\rangle$	$\frac{1}{2}\left(-\lvert {\rm g_I}{\rm u_I}\rangle - \lvert {\rm g_{II}}{\rm u_{II}}\rangle + \lvert {\rm g_I}{\rm u_{II}}\rangle - \lvert {\rm u_I}{\rm g_{II}}\rangle\right)$	$E^{(2)} - \frac{1}{8}J_{\rm H} - \frac{1}{2}I + (t_{\rm uu} + t_{\rm gg})$
	$\lvert\psi^{(2)}_{\rm u,t,4}\rangle =$	$\left\lvert \begin{matrix} \uparrow & \uparrow \\ - & - \end{matrix} \right\rangle$	$-\lvert {\rm u_I}{\rm u_{II}}\rangle$	$E^{(2)} - \varepsilon_{\rm g} + \varepsilon_{\rm u} + \frac{3}{4}U_{\rm g} - \frac{3}{4}U_{\rm u} - \frac{1}{2}U'$ $+\frac{3}{2}V_{\rm gg} - \frac{1}{2}V_{\rm uu} - \frac{1}{2}V_{\rm gu}$

ab initio Hamiltonian from the knowledge of the eigenvalues and wavefunctions. Such approach was originally developed for the situation with larger CI expansions in which effective parameters can be extracted by projecting those onto a model space.[11,12,42]

The MR-CI wavefunctions can be written as

$$|\Psi_j\rangle = \sum_i d_{ij}|\psi_i\rangle, \tag{4.13}$$

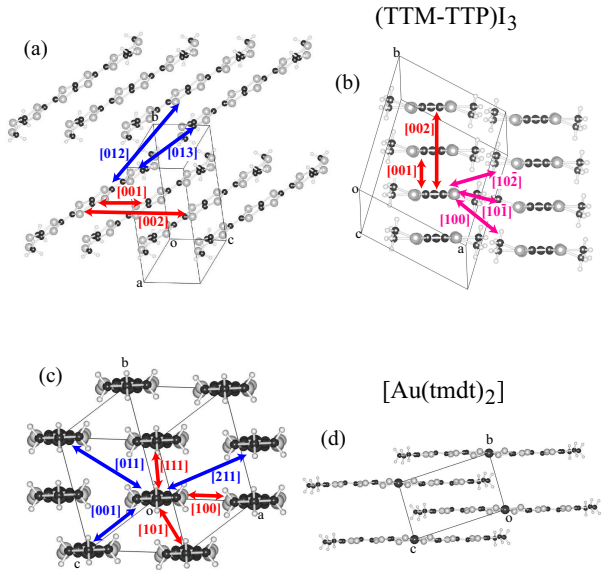

FIG. 4: Crystal structure of (TTM-TTP)I_3 [(a) and (b)], and crystal structure of [Au(tmdt)$_2$] [(c) and (d)]. The target pairs of two neighboring molecules are shown by the arrows, e.g., [001] and [002] in (TTM-TTP)I_3 represent the nearest-neighboring and next-nearest neighboring molecule pairs along the stacking c direction.

where the $|\psi_i\rangle$s are the configurations defined in Sec. IV B. From the MR-CI calculations, the energy eigenvalues $\{E_j\}$ and eigenfunctions $\{d_{ij}\}$ were obtained not only for the ground state but all the excited states contained in the model space. The Schrödinger equation can be formally expressed as

$$H\begin{pmatrix} d_{1j} \\ d_{2j} \\ \vdots \\ d_{Nj} \end{pmatrix} = E_j \begin{pmatrix} d_{1j} \\ d_{2j} \\ \vdots \\ d_{Nj} \end{pmatrix}, \tag{4.14}$$

where $j = 1, \ldots, N$, with N being the number of possible states. From $\{d_{ij}\}$, we define the unitary (orthogonal) matrix:

$$U = \begin{pmatrix} d_{11} & d_{12} & \cdots & d_{1N} \\ d_{21} & d_{22} & & d_{2N} \\ \vdots & & \ddots & \vdots \\ d_{N1} & & & d_{NN} \end{pmatrix}. \tag{4.15}$$

Together with the eigenvalues $\{E_j\}$, the Hamiltonian can be written as

$$H = U \begin{pmatrix} E_1 & & & \\ & E_2 & & \\ & & \ddots & \\ & & & E_N \end{pmatrix} U^{-1}. \tag{4.16}$$

Thus we can get not only the energy of each configuration, but also the off-diagonal matrix elements of the Hamiltonian.

D. Parameters mapping

Evidently, the full Hamiltonian is expressed on the basis $(\mathrm{g}_1, \mathrm{u}_1, \mathrm{g}_2, \mathrm{u}_2)$ whereas the model Hamiltonian is written on the molecular-based fragment MOs, $(\mathrm{g_I}, \mathrm{u_I}, \mathrm{g_{II}}, \mathrm{u_{II}})$. As can be seen from Fig. 2 and Eq. (4.9), the correspondence between the basis results in

$$c_{\mathrm{g}_1,\sigma} = \frac{1}{\sqrt{2}}(c_{\mathrm{g,I},\sigma} + c_{\mathrm{g,II},\sigma}), \tag{4.17a}$$

$$c_{\mathrm{u}_1,\sigma} = \frac{1}{\sqrt{2}}(-c_{\mathrm{g,I},\sigma} + c_{\mathrm{g,II},\sigma}), \tag{4.17b}$$

$$c_{\mathrm{g}_2,\sigma} = \frac{1}{\sqrt{2}}(-c_{\mathrm{u,I},\sigma} + c_{\mathrm{u,II},\sigma}), \tag{4.17c}$$

$$c_{\mathrm{u}_2,\sigma} = \frac{1}{\sqrt{2}}(c_{\mathrm{u,I},\sigma} + c_{\mathrm{u,II},\sigma}). \tag{4.17d}$$

By using these relations, we rewrite all the configurations into the molecular-based fragment MO basis, and derive the expression of Eq. (4.16) in terms of the parameters of the model Hamiltonian [Eq. (4.8)].

The zero-electron state is $|\psi^{(0)}\rangle = |\,0\rangle$, and the corresponding energy can be expressed in terms of model Hamiltonian as $E^{(0)} = \langle\psi^{(0)}|H_{\text{2-mol}}|\psi^{(0)}\rangle = (2E_0 + \Delta E_0) - 3(\varepsilon_\mathrm{g} + \varepsilon_\mathrm{u}) + 9(U_\mathrm{g} + U_\mathrm{u} + 4U')/8 + 9(V_\mathrm{gg} + V_\mathrm{uu} + 2V_\mathrm{gu})/4$.

By using Eq. (4.17), the one-electron states given in Eq. (4.12) are re-expressed as

$$|\psi^{(1)}_{\mathrm{g},1}\rangle = \frac{1}{\sqrt{2}}(|\mathrm{g_I}\rangle + |\mathrm{g_{II}}\rangle), \tag{4.18a}$$

$$|\psi^{(1)}_{\mathrm{u},1}\rangle = \frac{1}{\sqrt{2}}(-|\mathrm{g_I}\rangle + |\mathrm{g_{II}}\rangle), \tag{4.18b}$$

$$|\psi^{(1)}_{\mathrm{g},2}\rangle = \frac{1}{\sqrt{2}}(-|\mathrm{u_I}\rangle + |\mathrm{u_{II}}\rangle), \tag{4.18c}$$

$$|\psi^{(1)}_{\mathrm{u},2}\rangle = \frac{1}{\sqrt{2}}(|\mathrm{u_I}\rangle + |\mathrm{u_{II}}\rangle), \tag{4.18d}$$

where we have used the notation $|\mathrm{g_I}\rangle = c^\dagger_{\mathrm{g}_1,\uparrow}|0\rangle$ and so on.

By focusing on these four one-electron states, the extended Hubbard model Hamiltonian (4.8) can be expressed by the 4×4 matrix. The molecular-based fragment MO picture gives the following CI matrix expressed in the model space:

$$H_{\text{2-mol}} = \begin{pmatrix} E^{(1)}_\mathrm{g} & -t_\mathrm{gg} & \Delta\tilde{\varepsilon}_\mathrm{gu} & -t_\mathrm{gu} \\ -t_\mathrm{gg} & E^{(1)}_\mathrm{g} & t_\mathrm{gu} & -\Delta\tilde{\varepsilon}_\mathrm{gu} \\ \Delta\tilde{\varepsilon}_\mathrm{gu} & t_\mathrm{gu} & E^{(1)}_\mathrm{u} & -t_\mathrm{uu} \\ -t_\mathrm{gu} & -\Delta\tilde{\varepsilon}_\mathrm{gu} & -t_\mathrm{uu} & E^{(1)}_\mathrm{u} \end{pmatrix} \begin{matrix} |\mathrm{g_I}\rangle \\ |\mathrm{g_{II}}\rangle \\ |\mathrm{u_I}\rangle \\ |\mathrm{u_{II}}\rangle \end{matrix}, \tag{4.19}$$

where $E^{(1)}_\mathrm{g} = (E^{(0)} + \varepsilon_\mathrm{g} - 3U_\mathrm{g}/4 - 3U'/2 - 3V_\mathrm{gg}/2 - 3V_\mathrm{gu}/2)$, $E^{(1)}_\mathrm{u} = (E^{(0)} + \varepsilon_\mathrm{u} - 3U_\mathrm{u}/4 - 3U'/2 - 3V_\mathrm{uu}/2 - 3V_\mathrm{gu}/2)$, and $\Delta\tilde{\varepsilon}_\mathrm{gu} = (\Delta\varepsilon_\mathrm{gu} + 3X_\mathrm{g}/2 + 3X_\mathrm{u}/2)$. The intermolecular transfer integrals t_gg, t_uu, and t_gu are shown in Fig. 3. In terms of the basis given in Eq. (4.18), this CI matrix can be block diagonalized as

$$H_{2\text{-mol}} = \begin{pmatrix} E_{\rm g}^{(1)} - t_{\rm gg} & -\Delta\tilde{\varepsilon}_{\rm gu} - t_{\rm gu} & 0 & 0 \\ -\Delta\tilde{\varepsilon}_{\rm gu} - t_{\rm gu} & E_{\rm u}^{(1)} + t_{\rm uu} & 0 & 0 \\ 0 & 0 & E_{\rm g}^{(1)} + t_{\rm gg} & -\Delta\tilde{\varepsilon}_{\rm gu} + t_{\rm gu} \\ 0 & 0 & -\Delta\tilde{\varepsilon}_{\rm gu} + t_{\rm gu} & E_{\rm u}^{(1)} - t_{\rm uu} \end{pmatrix} \begin{matrix} |\psi_{\rm g,1}^{(1)}\rangle \\ |\psi_{\rm g,2}^{(1)}\rangle \\ |\psi_{\rm u,1}^{(1)}\rangle \\ |\psi_{\rm u,2}^{(1)}\rangle \end{matrix} . \tag{4.20}$$

Since the MOs are frozen to the ones obtained in the isolated molecule calculation, the off-diagonal elements $\langle\psi_{\rm g,1}^{(1)}|H_{2\text{-mol}}|\psi_{\rm g,2}^{(1)}\rangle$ and $\langle\psi_{\rm u,1}^{(1)}|H_{2\text{-mol}}|\psi_{\rm u,2}^{(1)}\rangle$ become non zero.

Similar implementations can be performed for the 2-electron case. The expressions of each configuration on the molecular-based fragment MO basis and the corresponding energies in terms of the extended Hubbard Hamiltonian are shown in Table II. We also analyze the off-diagonal components, and derive the CI matrix explicitly in terms of the parameters of the extended Hubbard Hamiltonian.

E. Results

Now we can evaluate the model parameters by relating the CI matrix obtained by the MR-CI calculations given in Eq. (4.16) and the CI matrix expressed in terms of the model Hamiltonian. In the extended Hubbard Hamiltonian [Eq. (4.8)], there are 17 parameters, including the intra-molecular interactions. In the two-electron case, 22 diagonal terms and 30 independent off-diagonal terms can be determined in the *ab initio* Hamiltonian (4.16). Interestingly, the intra-molecular interactions, $U_{\rm g}$, $U_{\rm u}$, U', and $J_{\rm H}$, are also obtained from the calculations for the two-molecule system. These values are consistent with the results in Table I.

For $[Au(tmdt)_2]$, the inter-molecular interactions are listed in Table III. From the data of transfer integrals, we see that the system exhibits three-dimensional character, in agreement with DFT-based calculations.[23] The estimated parameters for $\Delta\varepsilon_{\rm g}$, $\Delta\varepsilon_{\rm u}$, and $\Delta\varepsilon_{\rm gu}$ are also listed in Table III and are comparable to the energy difference $(\varepsilon_{\rm g}^0 - \varepsilon_{\rm u}^0) \approx 0.26$ eV. For (TTM-TTP)I_3, the inter-molecular interactions exhibit strong anisotropy, i.e., the inter-molecular interactions for the [001] molecule pair become largest compared with those for other pairs.[41] These features can be explained by noting that [001] is the stacking direction of TTM-TTP molecules and the two-molecule distance becomes much shorter for this face-to-face molecule pair. The parameters $\Delta\varepsilon_{\rm g}$ and $\Delta\varepsilon_{\rm u}$ for the ionic TTM-TTP^+ molecules are large in contrast to those for the neutral $[Au(tmdt)_2]$ molecules. Since these values are almost identical $\Delta\varepsilon_{\rm g} \simeq \Delta\varepsilon_{\rm u}$, we find that the g and u MOs are still quasi-degenerate in the crystal.

TABLE III: Estimated parameters for the neighboring $[Au(tmdt)_2]$ molecules. All energies are in eV.

direction	[100]	[111]	[101]	[211]	[001]	[011]
$t_{\rm gg}$	0.10	0.10	0.02	0.01	0.07	0.01
$t_{\rm uu}$	0.12	−0.19	−0.05	−0.02	−0.11	−0.02
$t_{\rm gu}$	0.00	−0.14	−0.03	−0.01	−0.09	−0.02
$V_{\rm gg}$	1.75	1.31	1.38	0.97	1.37	1.13
$V_{\rm uu}$	1.67	1.39	1.43	1.00	1.37	1.14
$V_{\rm gu}$	1.70	1.35	1.41	0.99	1.38	1.13
I	0.43	−0.29	−0.24	−0.11	−0.13	−0.09
$X_{\rm g}$	0.09	−0.56	−0.52	−0.28	−0.45	−0.31
$X_{\rm u}$	0.05	−0.58	−0.52	−0.29	−0.43	−0.31
$\Delta\varepsilon_{\rm g}$	0.26	−0.11	−0.06	−0.07	0.03	−0.01
$\Delta\varepsilon_{\rm u}$	0.20	−0.06	0.00	−0.05	0.07	0.02
$\Delta\varepsilon_{\rm gu}$	−0.10	0.21	0.19	0.04	0.31	0.12

It is known that the orbital exchange interaction term I accounts for dispersion interactions (i.e., van der Waals interactions) between pairs of molecules.[43–45] These correspond to instantaneous dipole-dipole interactions resulting from the local charge excitations $g_{\rm I} \to u_{\rm I}$ and $g_{\rm II} \to u_{\rm II}$ [see Eq. (4.6)], with the excitation energy ΔE. The dispersion interaction can be evaluated as $\sim -I^2/\Delta E$, and the typical amplitudes of the dispersion interaction are in the range -0.1 to -0.01 eV. In the present systems, the dispersion interactions for nearest-neighboring molecules are -0.24 eV for $[Au(tmdt)_2]_2$ and -0.08 eV for $[TTM\text{-}TTP^-]_2$. For the typical one-band system of the TTF molecules, we also evaluated the parameter $I = 0.19$ eV and found that the dispersion interaction is very weak (~ -0.006 eV). Such an observation can be ascribed to the fact that the present systems are very polarizable due to extended MOs.

In the way shown above, we determine all the possible model parameters uniquely for multi-orbital systems by taking the advantage of the wavefunction-based *ab initio* calculations. However, the resulting parameters shown here are bare values and the screening effects are not taken into account. A framework to project the effective model from large CI expansions has been developed where the electronic excitations involving valence and virtual MOs, i.e., so-called dynamic correlations, are taken into account.[11,12,42] With this scheme, one can access to accurate magnetic interactions, and simultaneously, transfer integral t, Coulomb repulsion U, and the direct exchange coupling, with the inclusion of these screening effects. For *atomic* orbitals in metal complexes, the screening effects to Coulomb repulsions are pronounced due to the localized orbital nature and also due to the presence of ligands, typically by a factor of 4 to 5.[12] It has been shown that this scheme is relevant to the analysis of pure organic

materials,[13,46] and the screening effects would be less important for larger molecules.[5] From the recent approaches based on DFT, where the *inter-molecular* screening effects in addition to the above *intra-molecular* screening effects are taken into account, the bare magnitudes for the Coulomb repulsions are reduced to at most a quarter.[5,8]

V. MODEL FOR CRYSTAL SYSTEM AND BAND STRUCTURE

In this section, we consider the crystal system and evaluate the band structure. The symmetry-breaking term $\Delta\varepsilon_{\rm gu}$ [Eq. (4.4)] disappears in the periodic crystal system. The full Hamiltonian is given by $H_{\rm cryst} = H^{\rm kin}_{\rm cryst} + H^{\rm int}_{\rm cryst}$ with

$$
\begin{aligned}
H^{\rm kin}_{\rm cryst} &= \sum_j (\varepsilon_{\rm g} n_{{\rm g},j} + \varepsilon_{\rm u} n_{{\rm u},j}) - \sum_{\langle i,j\rangle}\sum_\sigma t^{[n_a,n_b,n_c]}_{\rm gg} (c^\dagger_{{\rm g},i,\sigma} c_{{\rm g},j,\sigma} + {\rm h.c.}) - \sum_{\langle i,j\rangle}\sum_\sigma t^{[n_a,n_b,n_c]}_{\rm uu} (c^\dagger_{{\rm u},i,\sigma} c_{{\rm u},j,\sigma} + {\rm h.c.}) \\
&\quad - \sum_{\langle i,j\rangle}\sum_\sigma t^{[n_a,n_b,n_c]}_{\rm gu} (c^\dagger_{{\rm g},i,\sigma} c_{{\rm u},j,\sigma} - c^\dagger_{{\rm u},i,\sigma} c_{{\rm g},j,\sigma} + {\rm h.c.}), \qquad (5.1a) \\
H^{\rm int}_{\rm cryst} &= \sum_j \left\{ U_{\rm g} n_{{\rm g},j,\uparrow} n_{{\rm g},j,\downarrow} + U_{\rm u} n_{{\rm u},j,\uparrow} n_{{\rm u},j,\downarrow} + U' n_{{\rm g},j} n_{{\rm u},j} - J_{\rm H} \left[\boldsymbol{S}_{{\rm g},j} \cdot \boldsymbol{S}_{{\rm u},j} - \frac{1}{2} (c^\dagger_{{\rm g},j,\uparrow} c_{{\rm u},j,\uparrow} c^\dagger_{{\rm g},j,\downarrow} c_{{\rm u},j,\downarrow} + {\rm h.c.}) \right] \right\} \\
&\quad + \sum_{\langle i,j\rangle} V^{[n_a,n_b,n_c]}_{\rm gg} n_{{\rm g},i} n_{{\rm g},j} + \sum_{\langle i,j\rangle} V^{[n_a,n_b,n_c]}_{\rm uu} n_{{\rm u},i} n_{{\rm u},j} + \sum_{\langle i,j\rangle} V^{[n_a,n_b,n_c]}_{\rm gu} \left(n_{{\rm g},i} n_{{\rm u},j} + n_{{\rm u},i} n_{{\rm g},j} \right) \\
&\quad + \sum_{\langle i,j\rangle}\sum_{\sigma,\sigma'} I^{[n_a,n_b,n_c]} \left(c^\dagger_{{\rm g},i,\sigma} c_{{\rm u},i,\sigma} c^\dagger_{{\rm u},j,\sigma'} c_{{\rm g},j,\sigma'} + c^\dagger_{{\rm g},i,\sigma} c_{{\rm u},i,\sigma} c^\dagger_{{\rm g},j,\sigma'} c_{{\rm u},j,\sigma'} + {\rm h.c.} \right) \\
&\quad + \sum_{\langle i,j\rangle}\sum_\sigma X^{[n_a,n_b,n_c]}_{\rm g} \left[n_{{\rm g},i} \left(c^\dagger_{{\rm g},j,\sigma} c_{{\rm u},j,\sigma} + {\rm h.c.} \right) - \left(c^\dagger_{{\rm g},i,\sigma} c_{{\rm u},i,\sigma} + {\rm h.c.} \right) n_{{\rm g},j} \right] \\
&\quad + \sum_{\langle i,j\rangle}\sum_\sigma X^{[n_a,n_b,n_c]}_{\rm u} \left[n_{{\rm u},i} \left(c^\dagger_{{\rm g},j,\sigma} c_{{\rm u},j,\sigma} + {\rm h.c.} \right) - \left(c^\dagger_{{\rm g},i,\sigma} c_{{\rm u},i,\sigma} + {\rm h.c.} \right) n_{{\rm u},j} \right], \qquad (5.1b)
\end{aligned}
$$

where $\langle i,j\rangle$ denotes the combination of neighboring molecule pair and is assumed that i represents the molecule in a reference position while j the translated molecule by the vector $[n_a, n_b, n_c]$ shown in Fig. 4.

Next we examine the band structure for crystals by neglecting the correlation effects. In order to determine the energy levels, the crystal field effect arising from the $\Delta\varepsilon_{\rm g}$ and $\Delta\varepsilon_{\rm u}$ terms must be taken into account. We note that, for (TTM-TTP)I_3, the potential due to the counterion I_3^- should also be included in order to examine this crystal field effect quantitatively. In addition, the Hartree corrections from Eq. (5.1b) also contribute to the energy difference of MO level energies; however, these contributions would be small since the density operators in Hamiltonian are represented in the normal-ordered form [see Eq. (3.7)]. In the present analysis for [Au(tmdt)$_2$], we assign the MO level energies as $\varepsilon_{\rm g} \approx \varepsilon^0_{\rm g} + 2\Delta\varepsilon^{[100]}_{\rm g}$ and $\varepsilon_{\rm u} \approx \varepsilon^0_{\rm u} + 2\Delta\varepsilon^{[100]}_{\rm u}$, where the factor 2 reflects the coordination number, and we simply focus on the kinetic term [Eq. (5.1a)]. The resulting band structure for the [Au(tmdt)$_2$] crystal is shown in Fig. 5. The bandwidth obtained from the present analysis is overestimated in comparison with the result of DFT-based calculation for the periodic system,[22] however, qualitative behavior of the band structure is well reproduced. By taking advantage of the present scheme, we can elucidate the nature of the band structure, by setting the mixing term to zero, i.e., $t_{\rm gu} = 0$. Such a fictitious band structure is also shown in Fig. 5. We observe that the two bands overlap and mix in together by large mixing amplitude, supporting a multi-band system.

The band structure for (TTM-TTP)I_3 is also analyzed.[41] From an extended Hückel approach,[4] the overlap integrals between the neighboring molecules along the stacking direction were given by $S_{\rm gg} = -0.19 \times 10^{-3}$, $S_{\rm uu} = -26.22 \times 10^{-3}$, and $S_{\rm gu} = -12.92 \times 10^{-3}$. The small transfer integral $t_{\rm gg}$ and also the small overlap integral $S_{\rm gg}$ result from the tilted alignment of TTM-TTP molecules along the stacking direction in the crystal. We observe that the band built on the u MO is much wider than the one built on the g MO. The bandwidth for the u MO is ~ 1.2 eV while that for the g MO is ~ 0.3 eV. Finally, since the inter-orbital transfer integral $t^{[001]}_{\rm gu}$ ($= -0.13$ eV) is relatively large compared with $t_{\rm gg}$, the g MO band is strongly modified, while the u band is not much affected near the Fermi energy.

VI. FULL FRAGMENT DECOMPOSITION

In this section, we derive the effective model based on full fragment MOs, which is the most fundamental model to analyze the "intra-molecular" degree of freedom. The relevant fragment MOs are simply the left and right part of MOs, $\varphi_{\rm L}$ and $\varphi_{\rm R}$, where the center fragment is omitted due to its small

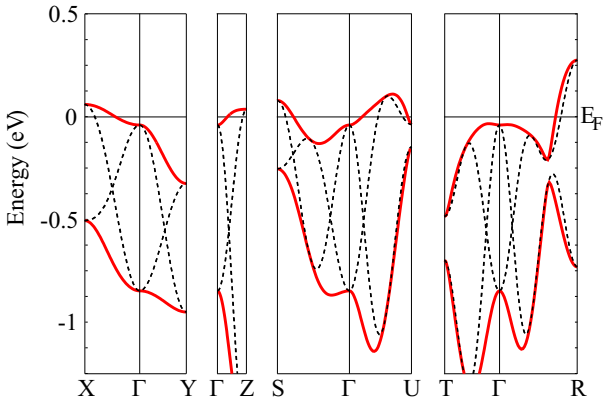

FIG. 5: Band structure of [Au(tmdt)$_2$] obtained from a parametrization based on our *ab initio* calculations, where $\Gamma = (0,0,0)$, $\mathrm{X} = (\pi,0,0)$, $\mathrm{Y} = (0,\pi,0)$, $\mathrm{Z} = (0,0,\pi)$, $\mathrm{S} = (\pi,\pi,0)$, $\mathrm{U} = (\pi,0,\pi)$, $\mathrm{T} = (0,\pi,\pi)$, and $\mathrm{R} = (\pi,\pi,\pi)$. The dotted curves represent the energy dispersion setting $t_{\mathrm{gu}} = 0$.

weight.[29] We denote the corresponding annihilation operators by $c_{\mathrm{L},j,\sigma}$ and $c_{\mathrm{R},j,\sigma}$. The operator correspondence between the original MOs and the fragment MOs basis is given by

$$c_{\mathrm{g},j,\sigma} = \frac{1}{\sqrt{2}}\left(-c_{\mathrm{L},j,\sigma} + c_{\mathrm{R},j,\sigma}\right), \tag{6.1a}$$

$$c_{\mathrm{u},j,\sigma} = \frac{1}{\sqrt{2}}\left(c_{\mathrm{L},j,\sigma} + c_{\mathrm{R},j,\sigma}\right). \tag{6.1b}$$

Let us mention that φ_L and φ_R are not orthogonal, but the overlap integral is very small.[29]

On the fragment MO basis, the model Hamiltonian for the crystal [Eq. (5.1)] can be re-expressed as $H_{\mathrm{cryst}} = H^{\mathrm{intramol}}_{\mathrm{cryst}} + H^{\mathrm{intermol}}_{\mathrm{cryst}}$ with

$$\begin{aligned}
&H^{\mathrm{intramol}}_{\mathrm{crystal}} \\
&= \varepsilon_0 \sum_j (n_{\mathrm{L},j} + n_{\mathrm{R},j}) \\
&- t_0 \sum_j \sum_\sigma (c^\dagger_{\mathrm{L},j,\sigma} c_{\mathrm{R},j,\sigma} + c^\dagger_{\mathrm{R},j,\sigma} c_{\mathrm{L},j,\sigma}) \\
&+ U \sum_j (n_{\mathrm{L},j,\uparrow} n_{\mathrm{L},j,\downarrow} + n_{\mathrm{R},j,\uparrow} n_{\mathrm{R},j,\downarrow}) \\
&+ V_0 \sum_j n_{\mathrm{L},j} n_{\mathrm{R},j} \\
&- J \sum_j \left[\boldsymbol{S}_{\mathrm{L},j} \cdot \boldsymbol{S}_{\mathrm{R},j} - \frac{1}{2}(c^\dagger_{\mathrm{L},j,\uparrow} c^\dagger_{\mathrm{L},j,\downarrow} c_{\mathrm{R},j,\downarrow} c_{\mathrm{R},j,\uparrow} + \mathrm{h.c.}) \right] \\
&+ X \sum_{j,\sigma} (n_{\mathrm{L},j,\sigma} + n_{\mathrm{R},j,\sigma})(c^\dagger_{\mathrm{L},j,\tilde{\sigma}} c_{\mathrm{R},j,\tilde{\sigma}} + \mathrm{h.c.}),
\end{aligned} \tag{6.2}$$

$$\begin{aligned}
&H^{\mathrm{intermol}}_{\mathrm{crystal}} \\
&= -\sum_{\langle i,j \rangle} \sum_\sigma t_1^{[n_a,n_b,n_c]} (c^\dagger_{\mathrm{R},i,\sigma} c_{\mathrm{L},j,\sigma} + \mathrm{h.c.}) \\
&- \sum_{\langle i,j \rangle} \sum_\sigma t_2^{[n_a,n_b,n_c]} (c^\dagger_{\mathrm{R},i,\sigma} c_{\mathrm{R},j,\sigma} + c^\dagger_{\mathrm{L},i,\sigma} c_{\mathrm{L},j,\sigma} + \mathrm{h.c.}) \\
&- \sum_{\langle i,j \rangle} \sum_\sigma t_3^{[n_a,n_b,n_c]} (c^\dagger_{\mathrm{L},i,\sigma} c_{\mathrm{R},j,\sigma} + \mathrm{h.c.}) \\
&+ \sum_{\langle i,j \rangle} V_1^{[n_a,n_b,n_c]} n_{\mathrm{R},i} n_{\mathrm{L},j} \\
&+ \sum_{\langle i,j \rangle} V_2^{[n_a,n_b,n_c]} (n_{\mathrm{L},i} n_{\mathrm{L},j} + n_{\mathrm{R},i} n_{\mathrm{R},j}) \\
&+ \sum_{\langle i,j \rangle} V_3^{[n_a,n_b,n_c]} n_{\mathrm{L},i} n_{\mathrm{R},j},
\end{aligned} \tag{6.3}$$

where $\tilde{\sigma} = \uparrow$ ($\downarrow$) for $\sigma = \downarrow$ ($\uparrow$). The parameters ε_0 and t_0 represent the energy level of the fragment MO and the inter-fragment transfer integral within the molecule. The parameter U represents the magnitude of the Coulomb repulsion between electrons within the fragment MOs, and V_0, J, and X denote the inter-fragment Coulomb repulsion, exchange interaction, and bond-density interactions within the molecule, respectively. The inter-molecular transfer integrals t_i ($i = 1,2,3$) and the inter-molecular Coulomb repulsions V_i ($i = 1,2,3$) are depicted in Fig. 6. The density operators are given in the normal-ordered form $n_{\mathrm{L/R},j,\sigma} = (c^\dagger_{\mathrm{L/R},j,\sigma} c_{\mathrm{L/R},j,\sigma} - \frac{3}{4})$ and the basis-set change leads to

$$\varepsilon_0 = \frac{1}{2}(\varepsilon_{\mathrm{g}} + \varepsilon_{\mathrm{u}}), \tag{6.4a}$$

$$t_0 = \frac{1}{2}(\varepsilon_{\mathrm{g}} - \varepsilon_{\mathrm{u}}), \tag{6.4b}$$

$$U = \frac{1}{4}(U_{\mathrm{g}} + U_{\mathrm{u}}) + \frac{1}{2}U' + \frac{5}{8}J_{\mathrm{H}}, \tag{6.4c}$$

$$V_0 = \frac{1}{8}(U_{\mathrm{g}} + U_{\mathrm{u}}) + \frac{3}{4}U' - \frac{5}{16}J_{\mathrm{H}}, \tag{6.4d}$$

$$J = \frac{1}{2}(U_{\mathrm{g}} + U_{\mathrm{u}}) - U' - \frac{1}{4}J_{\mathrm{H}}, \tag{6.4e}$$

$$X = \frac{1}{4}(-U_{\mathrm{g}} + U_{\mathrm{u}}), \tag{6.4f}$$

for the intra-molecular parameters. This kind of transformation was applied for simpler two-orbital systems.[47] Similarly, the inter-molecular interactions can be expressed as

$$t_1 = \frac{1}{2}(-t_{\mathrm{gg}} + t_{\mathrm{uu}} + 2t_{\mathrm{gu}}), \tag{6.5a}$$

$$t_2 = \frac{1}{2}(t_{\mathrm{gg}} + t_{\mathrm{uu}}), \tag{6.5b}$$

$$t_3 = \frac{1}{2}(-t_{\mathrm{gg}} + t_{\mathrm{uu}} - 2t_{\mathrm{gu}}), \tag{6.5c}$$

$$V_1 = \frac{1}{4}(V_{\mathrm{gg}} + V_{\mathrm{uu}}) + \frac{1}{2}V_{\mathrm{gu}} - I - X_{\mathrm{g}} - X_{\mathrm{u}}, \tag{6.5d}$$

$$V_2 = \frac{1}{4}(V_{\mathrm{gg}} + V_{\mathrm{uu}}) + \frac{1}{2}V_{\mathrm{gu}} + I, \tag{6.5e}$$

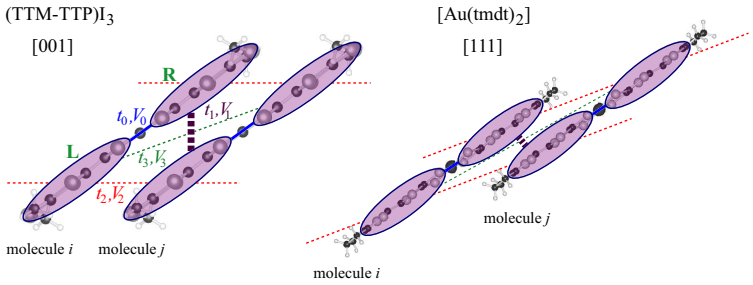

FIG. 6: The full-fragment-MO picture and the definition of parameters for (TTM-TTP)I_3 (left) and [Au(tmdt)$_2$] (right).

$$V_3 = \frac{1}{4}(V_{\rm gg}+V_{\rm uu})+\frac{1}{2}V_{\rm gu}-I+X_{\rm g}+X_{\rm u}, \quad (6.5f)$$

where the index $[n_a, n_b, n_c]$ is suppressed. The evaluated parameters are summarized in Table IV. It is worthwhile to note that the presence of the nontrivial orbital exchange interaction I and the bond-charge interaction $X_{\rm g}$ and $X_{\rm u}$ plays a crucial role to differentiate the Coulomb interactions, V_1, V_2, and V_3 in the fragment-MO picture.

The magnitudes of the Coulomb repulsion within the fragment, $U \simeq 5.30$ eV for TTM-TTP$^+$ and $U \simeq 5.26$ eV for [Au(tmdt)$_2$], are comparable with that for the TTF molecule $U_{\rm TTF} \simeq 6.2$ eV. For the inter-fragment transfer integrals, not only the nearest-neighbor Coulomb interactions but the long-range interactions have large amplitudes. In order to verify the fragment decomposition, we examine the distance dependence of the inter-fragment interactions. We define the inter-fragment distance r by the averaged inverse distance between the $N_{\rm S} = 6$ sulfur atoms in each fragment, by

$$\frac{1}{r} = \frac{1}{N_{\rm S}^2}\sum_{ij}\frac{1}{r_{ij}}, \quad (6.6)$$

where r_{ij} is the distance between the sulfur atoms. The r-dependences of the inter-fragment interaction V for [Au(tmdt)$_2$] and (TTM-TTP)I_3 are shown in Fig. 7 and in the supporting information.[41] The dotted curve denotes the bare Coulomb interactions $V(r) = 1/(4\pi\varepsilon_0 r)$, where ε_0 is the permittivity of vacuum. Thus, we conclude that V follows well the Coulomb law, and our fragment decomposition is verified from this evaluation of inter-fragment Coulomb repulsion. Incidentally, the fact that the intra-molecular Coulomb repulsion V_0 also follows well the Coulomb repulsion supports that the center fragment can be neglected.

From the data of inter-fragment transfer integrals, we find that the stacking TTM-TTP molecules ([001] direction) can be described as a two-leg ladder system, where the transfer integral along leg direction is t_2, while those along the rung direction are t_0 and t_1. It is worth noting that the inter-molecular transfer integral t_1 exceeds the intra-molecular transfer integral t_0. This implies that, as a possible origin to the insulating behavior at high temperature, electrons are localized on each t_1 bond, a reminiscence of the "dimer-Mott" state in the quarter-filled 1D systems.[48–50]

Here we discuss the low-temperature symmetry-broken states in (TTM-TTP)I_3 on the basis of the present model parameters. In (TTM-TTP)I_3, the intra-molecular charge ordering has been proposed from the Raman and x-ray experiments.[35–38] However, the charge pattern and the origin of the spin-singlet behavior have not been clarified yet. From a simple strong-coupling analysis, we can examine the energies of possible ordered states as shown in Fig. 8. We observe that the lowest-energy state is the ICO state ($E_{\rm ICO} = -1.47$ eV

TABLE IV: Estimated parameters for the inter-molecular interactions on the full-fragment MO basis for (TTM-TTP)I_3. The intra-molecular interactions are given by $\varepsilon_0 = -12.07$ eV, $t_0 = -0.17$ eV, $U = 5.30$ eV, $V_0 = 2.07$ eV, $J = 0.18$ eV, and $X = 0.05$ eV. All energies are in eV.

	[001]	[002]	[012]	[013]	[100]	[10$\bar{1}$]	[10$\bar{2}$]
t_1	−0.26	−0.01	−0.05	0.02	0.00	0.00	0.00
t_2	−0.17	0.00	0.01	0.00	0.00	0.00	0.00
t_3	0.01	0.00	0.00	0.00	0.00	−0.01	0.00
V_1	2.67	1.88	1.87	1.36	0.86	0.71	0.58
V_2	2.47	1.27	0.99	0.77	1.28	1.08	0.83
V_3	1.23	0.79	0.67	0.53	1.46	1.63	1.30

TABLE V: Estimated parameters for the inter-molecular interactions on the full-fragment MO basis for [Au(tmdt)$_2$]. The intra-molecular interactions are given by $\varepsilon_0 = -5.70$ eV, $t_0 = 0.19$ eV, $U = 5.26$ eV, $V_0 = 1.58$ eV, $J = 0.08$ eV, and $X = -0.01$ eV. All energies are in eV.

	[100]	[111]	[101]	[211]	[001]	[011]
t_1	0.01	−0.29	−0.07	−0.03	−0.18	−0.04
t_2	0.11	−0.04	−0.02	0.00	−0.02	0.00
t_3	0.01	0.00	0.00	0.00	0.00	0.00
V_1	1.13	2.79	2.69	1.67	2.39	1.85
V_2	2.14	1.06	1.16	0.87	1.24	1.04
V_3	1.41	0.50	0.62	0.54	0.61	0.60

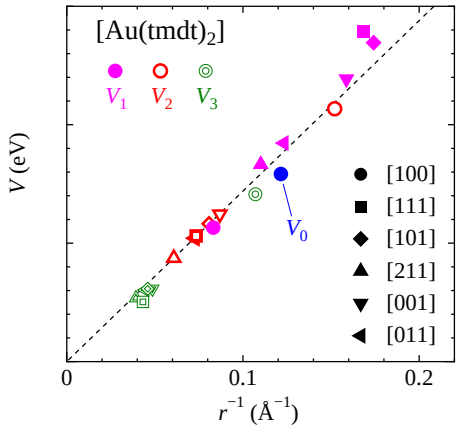

FIG. 7: The Coulomb repulsions as a function of inverse inter-fragment distance r^{-1} for $[Au(tmdt)_2]$. The results for (TTM-TTP)I_3 are shown in the supproting information.[41] The filled, open and double symbols represent V_1, V_2, and V_3, respectively. The repulsion between the L and R fragments within the molecule is characterized by V_0. The Coulomb repulsion within the fragment is $U \simeq 5.26$ eV. The dotted line represents the bare Coulomb repulsion a/r with $a \approx 14.4$ eV Å.

per molecule) in which the charge is disproportionated within each constitutive molecule. This ICO pattern is compatible with the $q_1 = (0, 0, 1/2)$ superstructure observed in the x-ray measurements.[31,32,38] From the evaluated model parameters, we expect that the super-exchange interaction along the t_1 bond becomes largest and it would play a crucial role to induce the spin-singlet state. On the basis of this finding, we infer that the non-magnetic insulating behavior observed at

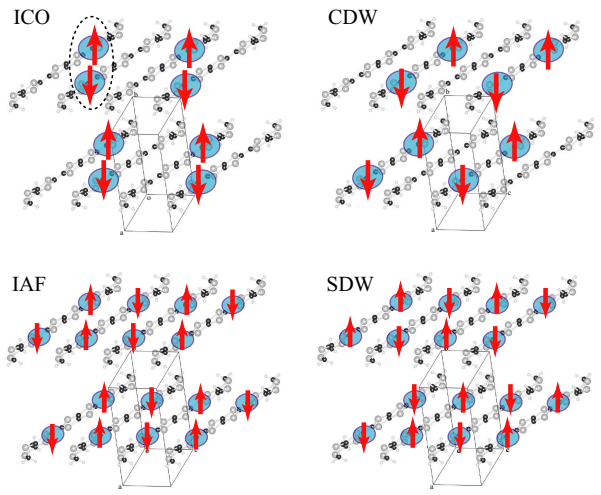

FIG. 8: Strong-coupling picture for several possible ordered states in (TTM-TTP)I_3 shown on the fragment-MO basis. Each circle (arrow) in the ICO and charge-density-wave (CDW) states represents one hole (spin), while that in the IAF and spin-density-wave (SDW) states represents half of hole (spin). In the ICO state, two holes surrounded by the dotted circle represent a spin-singlet pair. In the CDW state, two holes form a spin-singlet pair within a molecule.

low temperatures in (TTM-TTP)I_3[31–34] can be attributed to the spin-singlet formation on the $t_1^{[001]}$ bond (shown by the dotted circle in Fig. 8) with twofold periodicity along the stacking direction. Incidentally, we observe that the IAF state is almost degenerate with the ICO state, with the energy differences per molecule $E_{\rm IAF} - E_{\rm ICO} \approx 0.15$ eV, $E_{\rm SDW} - E_{\rm ICO} \approx 0.30$ eV, and $E_{\rm CDW} - E_{\rm ICO} \approx 1.19$ eV. Detailed analysis of possible symmetry-broken states described by the present Hamiltonian has been reported by using the mean-field approximation.[51]

From the optical measurement analysis, a nontrivial optical absorption band has been observed at ≈ 5000 cm^{-1}, corresponding to a charge transfer band.[37] It has been suggested that this band can only be observed under some electric fields polarized perpendicular to the stacking direction $E \perp c$. Furthermore its intensity is strongly enhanced at low temperatures. A possible scenario to explain this behavior is the following. In the ICO state, a characteristic charge excitation perpendicular to the stacking direction can be described with two holes localized on two adjacent fragments (see dotted circle in Fig. 8). If one considers a two-site two-electron system as a simplest model for this unit, the ground state is singlet with energy $E_0 = (U + V_1^{[001]})/2 - [(U - V_1^{[001]})^2/4 + 4(t_1^{[001]})^2]^{1/2}$. While the first-excited state with energy $E_1 = V_1$ represents an optically-forbidden spin transition, the unique optically-allowed transition involves the second-excited state with energy $E_2 = U$, representing a charge excitation. The corresponding excitation energy can be roughly estimated as 6800 cm^{-1} by using reduced Coulomb values (by a factor of 5).[5,8] Despite the localized character of this excitation description, our result is in relatively good agreement with experiments.

Similar analysis is performed for $[Au(tmdt)_2]$. For $[Au(tmdt)_2]$, we also find that the inter-molecular transfer integrals, $t_2^{[100]}$, $t_1^{[111]}$, and $t_1^{[001]}$ exceeds the intra-molecular transfer integral t_0. These features are qualitatively consistent with those obtained by fitting the DFT-based calculation.[25] In comparison to (TTM-TTP)I_3, we found that the two fragments connect by the $t_1^{[111]}$ bond form a strong dimer ($t_1^{[111]}/t_2^{[111]} \simeq 7.0$) in $[Au(tmdt)_2]$, while four fragments interact simultaneously in (TTM-TTP)I_3 where $t_1^{[001]}/t_2^{[001]} \simeq 1.5$. Due to this feature, the ICO state becomes unfavorable in $[Au(tmdt)_2]$. In addition, it has been pointed out that this system has a good nesting vector $q = (1/2, 0, 0)$ and the IAF state with this wave vector is stabilized.[23,25] If we restrict ourselves to the ordering with wave vector $q = (1/2, 0, 0)$, we observe from the strong-coupling analysis, that the ICO and CDW states are unstable with respect to the charge-uniform state in which each hole is localized on the $t_1^{[111]}$ bond. We note that this charge-uniform state is compatible to the IAF state if we take into account the antiferromagnetic interactions. The energy differences per molecule are $E_{\rm ICO} - E_{\rm IAF} \approx 0.07$ eV and $E_{\rm CDW} - E_{\rm IAF} \approx 0.14$ eV. More elaborate calculations based on our effective model should be carried out to clarify the origin of a huge magnetic moment suggested by the nuclear magnetic resonance measurement.[21]

VII. SUMMARY

In the present paper, we have proposed a scheme to determine the parameters of multi-orbital extended Hubbard model from the *ab initio* MR-CI calculations. To the best of our knowledge, this is the first theoretical work which aims at evaluating model parameters for a multi-orbital system. We have applied this method explicitly to the charge-transfer molecular conductor (TTM-TTP)I_3 and the single-component molecular conductor [Au(tmdt)$_2$]. By taking advantage of wavefunction-based calculations, the CI Hamiltonian matrix for the target model space was constructed, and all the model parameters were uniquely determined so as to reproduce the different matrix elements. By examining the band structure, we have verified the multi-band nature of these systems, since the SOMO- and HOMO-1-based bands overlap and these bands mix in together by the relatively large mixing amplitude. Furthermore, a full fragment decomposition picture leading to a parameter hierarchization has been justified by the observation that the inter-molecular Coulomb repulsions as well as the intra-molecular interaction V_0 follow well the Coulomb $1/r$ law. Our results strongly support that the ICO state experimentally-observed in (TTM-TTP)I_3 must be described by a multi-orbital picture.

Acknowledgments

The authors thank S. Ishibashi and H. Seo for the stimulating discussions at the early stage of the present work. MT thanks S. Yasuzuka, T. Kawamoto, T. Mori, and K. Yakushi for the fruitful discussions on the experimental aspects for the TTM-TTP compounds. MT and YO also thank L. Cano-Cortés, J. Merino, and K. Nakamura for discussions on the parameters evaluations of molecular solids. MT was supported by JSPS Institutional Program for Young Researcher Overseas Visits. YO and MLB were supported by the Grant-in-Aid for JSPS Fellows. This research was also partially supported by Grant-in-Aid for Scientific Research on Innovative Areas (20110002) from the Ministry of Education, Culture, Sports, Science and Technology, Japan.

[1] H. Seo, C. Hotta, and H. Fukuyama, Chem. Rev. **104**, 5005 (2004).
[2] H. Seo, J. Merino, H. Yoshioka, and M. Ogata, J. Phys. Soc. Jpn. **75**, 051009 (2006).
[3] T. Mori, Chem. Rev. **104**, 4947 (2004).
[4] T. Mori, A. Kobayashi, Y. Sasaki, H. Kobayashi, G. Saito, and H. Inokuchi, Bull. Chem. Soc. Jpn. **57**, 627 (1984).
[5] L. Cano-Cortés, A. Dolfen, J. Merino, J. Behler, B. Delley, K. Reuter, and E. Koch, Eur. Phys. J. B **56**, 173 (2007).
[6] E. Scriven and B. J. Powell, J. Chem. Phys. **130**, 104508 (2009).
[7] E. Scriven and B. J. Powell, Phys. Rev. B **80**, 205107 (2009).
[8] K. Nakamura, Y. Yoshimoto, T. Kosugi, R. Arita, and M. Imada, J. Phys. Soc. Jpn. **78**, 083710 (2009).
[9] H. C. Kandpal, I. Opahle, Y.-Z. Zhang, H. O. Jeschke, and R. Valentí, Phys. Rev. Lett. **103**, 067004 (2009).
[10] M. Imada and T. Miyake, J. Phys. Soc. Jpn. **79**, 112001 (2010).
[11] C. J. Calzado, J. Cabrero, J. P. Malrieu, and R. Caballol, J. Chem. Phys. **116**, 2728 (2002).
[12] C. J. Calzado, J. Cabrero, J. P. Malrieu, and R. Caballol, J. Chem. Phys. **116**, 3985 (2002).
[13] M. Vérot, J.-B. Rota, M. Kepenekian, B. L. Guennic, and V. Robert, Phys. Chem. Chem. Phys. **13**, 6657 (2011).
[14] A. Kobayashi, H. Tanaka, and H. Kobayashi, J. Mater. Chem. **11**, 2078 (2001).
[15] A. Kobayashi, E. Fujiwara, and H. Kobayashi, Chem. Rev. **104**, 5243 (2004).
[16] A. Kobayashi, Y. Okano, and H. Kobayashi, J. Phys. Soc. Jpn. **75**, 051002 (2006).
[17] H. Tanaka, Y. Okano, H. Kobayashi, W. Suzuki, and A. Kobayashi, Science **291**, 285 (2001).
[18] H. Tanaka, M. Tokumoto, S. Ishibashi, D. Graf, E. S. Choi, J. S. Brooks, S. Yasuzuka, Y. Okano, H. Kobayashi, and A. Kobayashi, J. Am. Chem. Soc. **126**, 10518 (2004).
[19] W. Suzuki, E. Fujiwara, A. Kobayashi, Y. Fujishiro, E. Nishibori, M. Takata, M. Sakata, H. Fujiwara, and H. Kobayashi, J. Am. Chem. Soc. **125**, 1486 (2003).
[20] B. Zhou, M. Shimamura, E. Fujiwara, A. Kobayashi, T. Higashi, E. Nishibori, M. Sakata, H. Cui, K. Takahashi, and H. Kobayashi, J. Am. Chem. Soc. **128**, 3872 (2006).
[21] Y. Hara, K. Miyagawa, K. Kanoda, M. Shimamura, B. Zhou, A. Kobayashi, and H. Kobayashi, J. Phys. Soc. Jpn. **77**, 053706 (2008).
[22] S. Ishibashi, H. Tanaka, M. Kohyama, M. Tokumoto, A. Kobayashi, H. Kobayashi, and K. Terakura, J. Phys. Soc. Jpn. **74**, 843 (2005).
[23] S. Ishibashi, K. Terakura, and A. Kobayashi, J. Phys. Soc. Jpn. **77**, 024702 (2008).
[24] C. Rovira, J. J. Novoa, J.-L. Mozos, P. Ordejón, and E. Canadell, Phys. Rev. B **65**, 081104 (2002).
[25] H. Seo, S. Ishibashi, Y. Okano, H. Kobayashi, A. Kobayashi, H. Fukuyama, and K. Terakura, J. Phys. Soc. Jpn. **77**, 023714 (2008).
[26] T. Mori, H. Inokuchi, Y. Misaki, T. Yamabe, H. Mori, and S. Tanaka, Bull. Chem. Soc. Jpn. **67**, 661 (1994).
[27] T. Mori, T. Kawamoto, J. Yamaura, T. Enoki, Y. Misaki, T. Yamabe, H. Mori, and S. Tanaka, Phys. Rev. Lett. **79**, 1702 (1997).
[28] S. Yasuzuka, K. Murata, T. Fujimoto, M. Shimotori, T. Kawamoto, T. Mori, M. Hedo, and Y. Uwatoko, J. Phys. Soc. Jpn. **75**, 053701 (2006).
[29] M.-L. Bonnet, V. Robert, M. Tsuchiizu, Y. Omori, and Y. Suzumura, J. Chem. Phys. **132**, 214705 (2010).
[30] M. Tsuchiizu, Y. Omori, Y. Suzumura, M.-L. Bonnet, V. Robert, S. Ishibashi, and H. Seo, J. Phys. Soc. Jpn. **80**, 013703 (2011).
[31] M. Maesato, Y. Sasou, S. Kagoshima, T. Mori, T. Kawamoto, Y. Misaki, and T. Yamabe, Synth. Met. **103**, 2109 (1999).
[32] N. Fujimura, A. Namba, T. Kambe, Y. Nogami, K. Oshima, T. Mori, T. Kawamoto, Y. Misaki, and T. Yamabe, Synth. Met. **103**, 2111 (1999).
[33] M. Onuki, K. Hiraki, T. Takahashi, D. Jinno, T. Kawamoto, T. Mori, T. Takano, and Y. Misaki, Synth. Met. **120**, 921 (2001).
[34] M. Onuki, K. Hiraki, T. Takahashi, D. Jinno, T. Kawamoto, T. Mori, K. Tanaka, and Y. Misaki, J. Phys. Chem. Sol. **62**, 405

(2001).
[35] K. Yakushi, R. Świetlik, K. Yamamoto, T. Kawamoto, T. Mori, Y. Misaki, and K. Tanaka, Synth. Met. **135-136**, 583 (2003).
[36] R. Świetlik, K. Yakushi, K. Yamamoto, T. Kawamoto, and T. Mori, J. Mol. Str. **704**, 89 (2004).
[37] R. Świetlik, K. Yakushi, K. Yamamoto, T. Kawamoto, and T. Mori, Synth. Met. **150**, 83 (2005).
[38] Y. Nogami, T. Kambe, N. Fujimura, K. Oshima, T. Mori, and T. Kawamoto, Synth. Met. **135-136**, 637 (2003).
[39] A. Szabo and N. Ostlund, *Modern Quantum Chemistry* (McGraw-Hill Book Company, 1989).
[40] G. Karlström, R. Lindh, P.-A. Malmqvist, B. O. Roos, U. Ryde, V. Veryazov, P.-O. Widmark, M. Cossi, B. Schimmelpfennig, P. Neogrady, and L. Seijo, Comp. Mater. Sci. **28**, 222 (2003).
[41] See supplementary material at http://dx.doi.org/10.1063/1.3678307 for the data of (TTM-TTP)I_3 and the model parameters of hydrogen molecule.
[42] C. Bloch, Nucl. Phys. **6**, 329 (1958).
[43] V. Robert, M. Képénékian, J. Rota, M.-L. Bonnet, and B. Guennic, *Computational Methods in Catalysis and Materials Science* (Wiley-VCH, Weinheim, 2009).
[44] F. London, Z. Phys. **63**, 245 (1930).
[45] O. Perraud, V. Robert, H. Gornitzka, A. Martinez, and J.-P. Dutasta, Angew. Chem. Int. Edit. **51**, 504, (2012).
[46] C. Calzado, C. Angeli, C. de Graaf, and R. Caballol, Theor. Chem. Acc. **128**, 505 (2011).
[47] V. Bonačić-Koutecký, J. Koutecký, and J. Michl, Angew. Chem. Int. Edit. **26**, 170 (1987).
[48] H. Seo and H. Fukuyama, J. Phys. Soc. Jpn. **66**, 1249 (1997).
[49] M. Tsuchiizu, H. Yoshioka, and Y. Suzumura, J. Phys. Soc. Jpn. **70**, 1460 (2001).
[50] M. Tsuchiizu and E. Orignac, J. Phys. Chem. Solids **63**, 1459 (2001).
[51] Y. Omori, M. Tsuchiizu, and Y. Suzumura, J. Phys. Soc. Jpn. **80**, 024707 (2011).